**Title: Lysosome Targeting Chimeras (LYTACs) for the Degradation of Secreted and Membrane Proteins**

**One Sentence Summary:** Chemically reprogrammed antibodies capable of bridging an antigen and a lysosomal shuttling receptor enable targeted protein degradation.

**Authors:** Steven M. Banik[1], Kayvon Pedram[1], Simon Wisnovsky[1], Nicholas M. Riley[1], Carolyn R. Bertozzi[1,2]*

**Affiliations:**
[1]Department of Chemistry, Stanford University, Stanford, California 94305, USA.
[2]Howard Hughes Medical Institute, Stanford, California 94305, USA.
*Correspondence should be addressed to C.R.B. (bertozzi@stanford.edu).

**Abstract:** Targeted protein degradation is a powerful strategy to address the canonically undruggable proteome. However, current technologies are limited to targets with cytosolically-accessible and ligandable domains. Here, we designed and synthesized conjugates capable of binding both a cell surface lysosome targeting receptor and the extracellular domain of a target protein. These lysosome targeting chimeras (LYTACs) consist of an antibody fused to agonist glycopeptide ligands for the cation-independent mannose-6-phosphate receptor (CI-M6PR). LYTACs enabled a CRISPRi knockdown screen revealing the biochemical pathway for CI-M6PR-mediated cargo internalization. We demonstrated that LYTACs mediate efficient degradation of Apolipoprotein-E4, epidermal growth factor receptor (EGFR), CD71, and programmed death-ligand 1 (PD-L1). LYTACs represent a modular strategy for directing secreted and membrane proteins for degradation in the context of both basic research and therapy.

**Main Text:** Most protein-directed therapeutics act by obstructing target function, as is the case with enzyme inhibitors and receptor blockers, or by recruiting immune effectors, as with many monoclonal antibody drugs. However, many potential therapeutic targets have molecular functions that are either incompletely understood or not readily druggable by these mechanisms (e.g., transcription factors, scaffolding proteins, aggregate-forming proteins, lipid carriers, mucins, orphan receptors, and polyfunctional molecules). Proteolysis targeting chimeras (PROTACs) (*1*, *2*) and conceptually related degradation platforms (e.g., dTAGs (*3*), Trim-Away (*4*), chaperone-mediated autophagy targeting (*5*) and SNIPERs(*6*)) have emerged as elegant strategies to address these canonically “undruggable” targets. PROTACs form a bridge between an E3 ubiquitin ligase and their target of interest, thereby facilitating ubiquitination and degradation by the proteasome (*7*). Despite their transformative power, state-of-the-art protein degradation technologies are, by their mechanism, fundamentally limited to targets with cytosolic domains, leaving secreted and many membrane proteins inaccessible. Reflecting ~40% of protein-encoding genes (*8*), secreted and membrane proteins play key roles in many disease states, including cancer, neurodegeneration, autoimmunity and infectious disease (*9*). Therefore, a general strategy for targeting secreted and plasma membrane proteins for degradation remains an unmet need that could dramatically impact human health.

Unlike the proteasomal pathway, the lysosomal pathway for protein degradation is not limited to proteins with intracellular domains. In addition, families of cell surface lysosomal targeting receptors (LTRs) have been discovered which facilitate transport of proteins to lysosomes (*10*). We hypothesized that chimeric molecules capable of binding both a cell surface LTR and an extracellular protein would induce internalization and lysosomal degradation of the target.

The prototypical LTR is the cation-independent mannose-6-phosphate receptor (CI-M6PR, also called IGF2R), which endogenously transports proteins bearing N-glycans capped

with mannose-6-phosphate (M6P) residues to lysosomes (*11*). The receptor cycles constitutively between endosomes, the cell surface, and the Golgi complex. Upon engagement by multivalent ligands, CI-M6PR shuttles cargo efficiently to prelysosomal compartments where a lower pH allows cargo to dissociate and progress to the lysosome while CI-M6PR recycles. Based on its ability to efficiently deliver cargo to lysosomes and its widespread tissue expression, CI-M6PR has been exploited to deliver therapeutic enzymes for treatment of lysosomal storage disorders (*12*). Here, we present the lysosome targeting chimera (LYTAC) platform, which enables depletion of secreted and membrane proteins via a mechanism of action that is orthogonal and complementary to existing technologies (Fig. 1A). Herein, LYTACs comprise antibodies conjugated with agonist multivalent glycopolypeptide ligands for CI-M6PR. We show that LYTACs can be used as biochemical probes to study receptor trafficking and protein degradation, and are capable of degrading both secreted and membrane proteins of therapeutic interest.

In our effort to develop CI-M6PR agonist ligands, we leveraged precedents from work aimed at enhancing lysosomal enzyme replacement therapies and drug delivery platforms. This prior work included biosynthetic engineering of M6P-bearing glycans (*13*) as well as chemical synthesis of oligomeric M6P-containing scaffolds (*14*). A recurring design parameter from these studies was the requirement of ligand multivalency to achieve optimal CI-M6PR agonism (*15*–*17*). Prior work had also revealed that the 6-phosphoester can undergo hydrolysis in human serum (*18*), leading to rapid endocytosis by macrophages bearing mannose receptors (*19*). We reasoned that *N*-carboxyanhydride (NCA)-derived glycopolypeptides (*20*) bearing multiple serine-*O*-mannose-6-phosphonate (M6Pn) residues would enable multivalent presentation on a biocompatible, phosphatase-inert (*21*), and modular scaffold. We synthesized M6Pn glycopolypeptides starting with conversion of mannose pentaacetate to M6Pn-NCA **1** in 13 steps (Fig. 1B). Subsequent copolymerization of **1** and alanine-NCA (1:1 ratio, for the purpose of spacing and polymerization kinetics) provided access to M6Pn glycopolypeptides (post-deprotection Đ = 1.3-1.5). The living nature of NCA polymerization allowed us to generate M6Pn glycopolypeptides of various lengths; for this study we made short (20 M6Pn) and long (90 M6Pn) variants to test in protein degradation assays. We also synthesized the corresponding M6P-containing copolymers bearing the natural phosphorylated glycan structure (Fig. S1), as well as copolymers with similar molecular weights and dispersities to those obtained with M6Pn monomers.

To demonstrate the feasibility of CI-M6PR-driven LYTACs, we designed an assay to measure uptake of NeutrAvidin-647 (NA-647) using conjugates comprising biotin N-terminally fused to glycopolypeptides (Fig. 1C). Additionally, we synthesized and biotinylated poly(GalNAc), and poly(Mannose) as control polymers (Fig. 1D and Fig. S2). K562 cells were incubated with NA-647 or NA-647 and biotinylated glycopolypeptide for 1 hour, then washed and analyzed by flow cytometry. Co-incubation with M6P and M6Pn polymers increased cellular fluorescence 5-6 fold over background, with only minor differences in uptake efficiency observed as a result glycopolypeptide length (short versus long, Fig. 1E). M6Pn-polymers performed equivalently or superior to M6P polymers of similar length, while incubation with mannose or GalNAc containing glycopolypeptides had no effect. NA-647 uptake mediated by poly(M6Pn) was attenuated by co-incubation with excess exogenous M6P. Further, uptake remained continuous over time (Fig. S3), consistent with surface receptor recycling acting as the rate-limiting step (*22*). Note that AF647 is reported to be stable in endosomes and lysosomes, consistent with steadily increasing fluorescent signal arising from intracellular fluorophore accumulation (*23*). In addition, live cell fluorescence microscopy revealed that AF647 signal co-localized with acidic endosomes and lysosomes after just 1 hour (Fig. 1F, Figs. S4–S5). Finally, biotin LYTACs mediated NA-647 uptake in a variety of cell lines, including those derived from breast cancer, cervical cancer, lymphoma, and leukemia, demonstrating the generality of CI-M6PR-targeting (Fig. 1G).

We performed a CRISPRi pooled genetic screen with the aim of identifying genes whose knockdown ablated intracellular delivery of LYTAC-conjugated NA-647 (*24*, *25*) (Fig. 2A). K562

cells expressing dCas9-KRAB were transduced with a genome-wide library of CRISPRi sgRNAs and incubated with LYTAC and NA-647. A population of cells exhibiting a significant decrease in NA-647 labeling was isolated by fluorescence-activated cell sorting (FACS). Next-Gen sequencing was performed to identify sgRNAs constitutively overrepresented in this population. Guide RNAs to CI-M6PR were highly enriched in the sorted pool, providing unbiased confirmation of selective receptor targeting (Fig. 2B, full dataset available in Supplementary Data 1). Other significantly enriched guides (FDR < 5%) targeted genes that regulate endosomal acidification, vesicle trafficking, endosome-lysosome fusion, and clathrin-dependent endocytosis (Fig. 2C), consistent with a CI-M6PR-driven endocytic pathway to lysosomes (*11*). Components of the exocyst complex, which is reported to mediate vesicle localization to the plasma membrane (*26*), were also identified as essential for M6Pn-mediated delivery of NA-647. We hypothesized that the exocyst complex could be involved in cell surface presentation of CI-M6PR, a biochemical pathway which has yet to be elucidated (*11*). We performed CRISPRi knockdown of EXOC1 and EXOC2 in K562 cells using CRISPRi library guides and measured cell-surface CI-M6PR levels by flow cytometry. Strikingly, we observed a 60% decrease in cell surface CI-M6PR (Fig. 2D). We replicated these results in HeLa cells (75% decrease, Fig. 2E), and found that total CI-M6PR as read out by Western blot did not change upon knockdown of EXOC1 in either cell line (Fig. 2F and Fig. 2G, respectively). Further, no change in surface expression of epidermal growth factor receptor (EGFR) in HeLa cells was observed (Fig. S6), indicating global cell surface protein trafficking remained unperturbed. Together these data indicate that surface presentation of CI-M6PR is mediated in part by the exocyst complex, and more broadly, that LYTACs can be used to study the molecular pathways involved in cell surface receptor regulation.

We next sought to determine if conjugation of a poly(M6Pn)-bearing glycopeptide to an antibody would reprogram the antibody to rapidly direct extracellular agents to the lysosome. As proof-of-principle, we non-specifically labeled lysines on a polyclonal anti-mouse IgG with bicyclononyne-NHS (BCN-NHS), and subsequently conjugated this antibody to azide-terminated glycopolypeptides via Cu-free strain-promoted azide-alkyne cycloaddition (Fig. 3A), generating LYTAC **Ab-1**. The conjugation reaction was readily monitored by native gel electrophoresis as covalent attachment of the highly anionic polypeptides caused a characteristic enhancement in migration compared to non-charged polypeptide-conjugated antibodies (i.e. GalNAc) (Fig. 3B). Incubation of K562 cells with mouse IgG labeled with AlexaFluor-488 (AF488) and **Ab-1** (Fig. 3C), resulted in a 40-fold increase in lysosomal AF488 signal relative to controls (Fig 3D and Fig. S7).

Given that **Ab-1** efficiently trafficked IgG molecules to lysosomes, we reasoned it could function as a LYTAC for a primary IgG antibody bound to its antigen (Fig. 3E). Co-incubation of cells with mCherry, mouse-anti mCherry, and **Ab-1** resulted in 10-100-fold increases in uptake relative to non-M6Pn bearing antibodies in all cell lines tested (Fig. 3 F–H). To expand this strategy to a clinically relevant target, we chose Apolipoprotein E4 (ApoE4), which has been implicated in the pathogenesis of neurodegenerative disease (*27*). A 13-fold increase in uptake was observed using **Ab-1** along with a mouse-anti-ApoE4 primary antibody (Fig. 3I), with uptake continuous over the course of the incubation (Fig. 3J). Co-localization of AF647 signal with lysosomes was observed at both 1 and 24 hours (Fig. S8), replicating our findings with NeutrAvidin and mCherry. Importantly, non-specific inhibition of serine and cysteine proteases using leupeptin resulted in accumulation of intracellular AF647-labeled ApoE (ApoE4-647), which was substantially increased in the presence of anti-ApoE4 with **Ab-1** (Fig. 3K and Fig. S9). These data demonstrate that LYTAC-mediated target enrichment at the lysosome is coupled with increased target degradation. More broadly, conjugation of a lysosomal targeting ligand to an antibody can reprogram the antibody to direct an extracellular antigen for degradation.

We next asked if LYTACs could be used to accelerate the degradation of membrane-associated extracellular proteins. In principle, this requires simultaneous binding of a surface-associated protein and stimulation of CI-M6PR, an interaction which would also benefit from increased effective molarity upon target binding. EGFR, a known driver of cancer proliferation,

which can perform multiple scaffolding functions regardless of kinase inhibition, served as the first target. LYTACs constructed using cetuximab (ctx), an FDA-approved EGFR-blocking antibody, were generated using a similar scheme to **Ab-1** (Fig. 4A). HeLa cells were incubated for 24 hours with 100 nM ctx, ctx functionalized with either long or short M6Pn glycopolypeptides, or GalNAc-functionalized ctx as a control (Fig. 4B). Cells were then lysed and assayed for total EGFR levels by Western blot (Fig. 4C). Substantial degradation of EGFR was observed only with ctx conjugates bearing M6Pn glycopolypeptides (>70% degradation, comparable to EGF-induced downregulation), while no change in CI-M6PR levels were observed. There was no apparent difference in degradation ability between LYTACs bearing short or long M6Pn glycopolypeptides. Analogous results were obtained with concentrations of ctx-M6Pn between 100 nM and 10 nM (Fig. S10). To confirm that depletion of EGFR was mediated by CI-M6PR, we compared the degrading ability of ctx-M6Pn **Ab-2** (Fig. S11) to unmodified ctx in dCas9-KRAB HeLa lines stably expressing a non-targeting or CI-M6PR-targeting sgRNA. Accelerated degradation of EGFR was only observed in non-targeting sgRNA-expressing HeLa cells, while knockdown of CI-M6PR completely abrogated the degradation ability of **Ab-2** (Fig. 4D). EGFR degradation reached maximum between 12-24 hours and persisted for at least 72 hours (Fig. S12). To rule out the possibility that EGFR crosslinking by ctx contributed to target downregulation (*28*, *29*), we digested ctx with papain to obtain ctx-Fab, a monovalent binder of EGFR, and conjugated it to poly(M6Pn-co-Ala) to generate **Fab-1** (Fig. 4E). **Fab-1** accelerated degradation of EGFR in a CI-M6PR-dependent manner to levels comparable with **Ab-2** (Fig. 4F), demonstrating that monovalent binders can be used as LYTACs. In a mixed cell assay with HeLa (CI-M6PR$^+$EGFR$^+$) and Jurkat (CI-M6PR$^+$EGFR$^-$) cells, the ctx-M6Pn conjugate exhibited a similar binding profile to ctx alone, suggesting that LYTACs with dual affinities for target and CI-M6PR can maintain high on-target specificity (Fig. S13). EGFR degradation was also observed in breast cancer (BT474, MDA-MB-361) and lung cancer (A549) cell lines (Fig. S14).

Next, proteome-wide characterization of LYTAC degradation specificity was evaluated via quantitative mass spectrometry analysis of cells treated with ctx or **Ab-2**. Significant reduction of EGFR levels was effected by **Ab-2**, while ctx did not affect EGFR levels significantly (Fig. 4G). CI-M6PR levels were unchanged, further supporting catalytic CI-M6PR-mediated degradation of EGFR. Changes in the expression levels of other proteins as a result of EGFR degradation were also observed (Fig. S15, full dataset in Supplementary Data 2). These co-degraded proteins may represent EGFR interaction partners or co-regulated molecules. For example, treatment with **Ab-2** caused significant downregulation of CD99, dihydropteridine reductase, 7,8-dihydro-8-oxoguanine triphosphatase, and transcription factor Dp-1, and resulted in upregulation of glucose-1,6-bisphosphate synthase and COPRS. While the precise mechanism for these changes remains to be elucidated, these data suggest that LYTACs may provide a new means to monitor cellular changes in response to protein degradation.

To demonstrate the generality of the LYTAC platform, we targeted several additional membrane-associated proteins for degradation. CD71 (transferrin receptor-1), a therapeutic cancer target progressing to clinical trials, is known to cycle between early endosomes and the cell surface, avoiding trafficking to the lysosome for degradation (*30*). Upon incubation of Jurkat cells with a mouse-anti-CD71 antibody and **Ab-1** (Fig. 4H), significant degradation of CD71 was observed (>80%, Fig. 4I). Note the anti-CD71 antibody alone is reported to induce partial CD71 downregulation (*31*). After 24 hours incubation, cells treated with anti-CD71 and **Ab-1** exhibited a decrease in transferrin-647 uptake compared to no treatment or treatment with non-M6Pn bearing antibodies (Fig. 4J), highlighting the functional consequences of target degradation in this system.

Finally, we investigated whether LYTACs could degrade PD-L1, a driver of cancer cell immune evasion. In order for PD-L1 to undergo accelerated degradation, the LYTAC must override the PD-L1 recycling pathway (*32*). MDA-MB-231 cells, which are PD-L1 positive, were treated with anti-PD-L1, anti-PD-L1 functionalized with GalNAc glycopolypeptides, or anti-PD-L1-

M6Pn LYTAC (**Ab-3**, Fig. S16). Treatment with **Ab-3** resulted in a significant decrease (average 33%) in cell-surface PD-L1 levels compared to unfunctionalized anti-PD-L1 or anti-PD-L1-poly(GalNAc) (Fig. 4K); the observed decrease was sustained over the course of 72 hours. At 48 hours, PD-L1 levels were reduced only in cells treated with **Ab-3,** as assayed by Western blot (Fig. 4L). As MDA-MB-231 express low levels of CI-M6PR, we next tested degradation of PD-L1 in the Hodgkin's lymphoma cell line HDLM-2 which expresses higher levels of CI-M6PR. After 36 hours, 50% downregulation of PD-L1 was observed (Fig. 4M). Together, these data demonstrate proof-of-principle that LYTACs can alter the endogenous recycling programs of cell-surface proteins and accelerate their lysosomal degradation.

In summary, LYTACs are a platform for targeting extracellular molecules directly for lysosomal degradation. The success of a particular LYTAC likely results from a combination of factors, including the endogenous kinetics of protein trafficking and turnover, amount of surface localization, inherent susceptibility to lysosomal transportation through clathrin-mediated endocytosis, and stoichiometry relative to the lysosome targeting receptor. While the LYTACs described above take advantage of CI-M6PR, in principle other recycling receptors could be coopted. We anticipate the chemical tunability and modularity of LYTACs will offer new opportunities in targeted protein degradation for both research and translational applications.

**References**


1. K. M. Sakamoto *et al.*, Protacs: Chimeric molecules that target proteins to the Skp1–Cullin–F box complex for ubiquitination and degradation. *Proc. Natl. Acad. Sci.* **98**, 8554–8559 (2001).

2. G. E. Winter *et al.*, Phthalimide conjugation as a strategy for in vivo target protein degradation. *Science*. **348**, 1376–1381 (2015).

3. B. Nabet *et al.*, The dTAG system for immediate and target-specific protein degradation. *Nat. Chem. Biol.* **14**, 431 (2018).

4. D. Clift *et al.*, A Method for the Acute and Rapid Degradation of Endogenous Proteins. *Cell*. **171**, 1692-1706.e18 (2017).

5. X. Fan, W. Y. Jin, J. Lu, J. Wang, Y. T. Wang, Rapid and reversible knockdown of endogenous proteins by peptide-directed lysosomal degradation. *Nat. Neurosci.* **17**, 471–480 (2014).

6. M. Naito, N. Ohoka, N. Shibata, SNIPERs—Hijacking IAP activity to induce protein degradation. *Drug Discov. Today Technol.* (2019), doi:10.1016/j.ddtec.2018.12.002.

7. G. M. Burslem, C. M. Crews, Small-Molecule Modulation of Protein Homeostasis. *Chem. Rev.* **117**, 11269–11301 (2017).

8. M. Uhlén *et al.*, Tissue-based map of the human proteome. *Science*. **347**, 1260419 (2015).

9. K. J. Brown *et al.*, The human secretome atlas initiative: Implications in health and disease conditions. *Biochim. Biophys. Acta*. **1834**, 2454–2461 (2013).

10. M. F. Coutinho, M. J. Prata, S. Alves, A shortcut to the lysosome: The mannose-6-phosphate-independent pathway. *Mol. Genet. Metab.* **107**, 257–266 (2012).

11. P. Ghosh, N. M. Dahms, S. Kornfeld, Mannose 6-phosphate receptors: new twists in the tale. *Nat. Rev. Mol. Cell Biol.* **4**, 202–213 (2003).

12. M. Gary-Bobo, P. Nirdé, A. Jeanjean, A. Morère, M. Garcia, Mannose 6-phosphate receptor targeting and its applications in human diseases. *Curr. Med. Chem.* **14**, 2945–2953 (2007).

13. L. Liu, W.-S. Lee, B. Doray, S. Kornfeld, Engineering of GlcNAc-1-Phosphotransferase for Production of Highly Phosphorylated Lysosomal Enzymes for Enzyme Replacement Therapy. *Mol. Ther. - Methods Clin. Dev.* **5**, 59–65 (2017).

14. Y. Zhu *et al.*, Conjugation of Mannose 6-Phosphate-containing Oligosaccharides to Acid α-Glucosidase Improves the Clearance of Glycogen in Pompe Mice. *J. Biol. Chem.* **279**, 50336–50341 (2004).

15. L. Beljaars *et al.*, Albumin modified with mannose 6-phosphate: A potential carrier for selective delivery of antifibrotic drugs to rat and human hepatic stellate cells. *Hepatology*. **29**, 1486–1493 (1999).

16. D. B. Berkowitz, G. Maiti, B. D. Charette, C. D. Dreis, R. G. MacDonald, Mono- and Bivalent Ligands Bearing Mannose 6-Phosphate (M6P) Surrogates: Targeting the M6P/Insulin-Like Growth Factor II Receptor. *Org. Lett.* **6**, 4921–4924 (2004).

17. S. Das, N. Parekh, B. Mondal, S. S. Gupta, Controlled Synthesis of End-Functionalized Mannose-6-phosphate Glycopolypeptides for Lysosome Targeting. *ACS Macro Lett.* **5**, 809–813 (2016).

18. A. Jeanjean, M. Garcia, A. Leydet, J.-L. Montero, A. Morère, Synthesis and receptor binding affinity of carboxylate analogues of the mannose 6-phosphate recognition marker. *Bioorg. Med. Chem.* **14**, 3575–3582 (2006).

19. W. S. Sly *et al.*, Enzyme therapy in mannose receptor-null mucopolysaccharidosis VII mice defines roles for the mannose 6-phosphate and mannose receptors. *Proc. Natl. Acad. Sci.* **103**, 15172–15177 (2006).

20. J. R. Kramer, B. Onoa, C. Bustamante, C. R. Bertozzi, Chemically tunable mucin chimeras assembled on living cells. *Proc. Natl. Acad. Sci.* **112**, 12574–12579 (2015).

21. A. Jeanjean *et al.*, Synthesis of new sulfonate and phosphonate derivatives for cation-independent mannose 6-phosphate receptor targeting. *Bioorg. Med. Chem. Lett.* **18**, 6240–6243 (2008).

22. T. E. Ritter, O. Fajardo, H. Matsue, R. G. Anderson, S. W. Lacey, Folate receptors targeted to clathrin-coated pits cannot regulate vitamin uptake. *Proc. Natl. Acad. Sci.* **92**, 3824–3828 (1995).

23. D. E. Johnson, P. Ostrowski, V. Jaumouillé, S. Grinstein, The position of lysosomes within the cell determines their luminal pH. *J Cell Biol*. **212**, 677–692 (2016).

24. M. Kampmann, M. C. Bassik, J. S. Weissman, Functional genomics platform for pooled screening and generation of mammalian genetic interaction maps. *Nat. Protoc.* **9**, 1825–1847 (2014).

25. M. A. Horlbeck *et al.*, Compact and highly active next-generation libraries for CRISPR-mediated gene repression and activation. *eLife*. **5**, e19760 (2016).

26. M. R. Heider, M. Munson, Exorcising the Exocyst Complex. *Traffic*. **13**, 898–907 (2012).

27. Y. Yamazaki, M. M. Painter, G. Bu, T. Kanekiyo, Apolipoprotein E as a Therapeutic Target in Alzheimer's Disease: A Review of Basic Research and Clinical Evidence. *CNS Drugs*. **30**, 773–789 (2016).

28. J. Y. Li *et al.*, A Biparatopic HER2-Targeting Antibody-Drug Conjugate Induces Tumor Regression in Primary Models Refractory to or Ineligible for HER2-Targeted Therapy. *Cancer Cell*. **29**, 117–129 (2016).

29. J. B. Spangler *et al.*, Combination antibody treatment down-regulates epidermal growth factor receptor by inhibiting endosomal recycling. *Proc. Natl. Acad. Sci.* **107**, 13252–13257 (2010).

30. Y. Shen *et al.*, Transferrin receptor 1 in cancer: a new sight for cancer therapy. *Am. J. Cancer Res.* **8**, 916–931 (2018).

31. A. M. Weissman, R. D. Klausner, K. Rao, J. B. Harford, Exposure of K562 cells to anti-receptor monoclonal antibody OKT9 results in rapid redistribution and enhanced degradation of the transferrin receptor. *J. Cell Biol.* **102**, 951–958 (1986).

32. M. L. Burr *et al.*, CMTM6 maintains the expression of PD-L1 and regulates anti-tumour immunity. *Nature*. **549**, 101–105 (2017).

33. W. B. Cowden, Phosphosugars and phosphosugar-containing compounds having anti-inflammatory activity (2001), (available at https://patents.google.com/patent/US6294521B1/en).

34. K. Lin, A. M. Kasko, Effect of Branching Density on Avidity of Hyperbranched Glycomimetics for Mannose Binding Lectin. *Biomacromolecules*. **14**, 350–357 (2013).

35. M. N. Zhou *et al.*, N-Carboxyanhydride Polymerization of Glycopolypeptides That Activate Antigen-Presenting Cells through Dectin-1 and Dectin-2. *Angew. Chem. Int. Ed Engl.* **57**, 3137–3142 (2018).

36. W. Li *et al.*, MAGeCK enables robust identification of essential genes from genome-scale CRISPR/Cas9 knockout screens. *Genome Biol.* **15**, 554 (2014).

37. E. Eden, R. Navon, I. Steinfeld, D. Lipson, Z. Yakhini, GOrilla: a tool for discovery and visualization of enriched GO terms in ranked gene lists. *BMC Bioinformatics*. **10**, 48 (2009).

38. A. S. Hebert *et al.*, Improved Precursor Characterization for Data-Dependent Mass Spectrometry. *Anal. Chem.* **90**, 2333–2340 (2018).

39. S. Tyanova, T. Temu, J. Cox, The MaxQuant computational platform for mass spectrometry-based shotgun proteomics. *Nat. Protoc.* **11**, 2301–2319 (2016).

40. J. Cox *et al.*, Andromeda: a peptide search engine integrated into the MaxQuant environment. *J. Proteome Res.* **10**, 1794–805 (2011).

41. J. E. Elias, S. P. Gygi, Target-decoy search strategy for increased confidence in large-scale protein identifications by mass spectrometry. *Nat. Methods*. **4**, 207–214 (2007).

42. J. Cox *et al.*, Accurate proteome-wide label-free quantification by delayed normalization and maximal peptide ratio extraction, termed MaxLFQ. *Mol. Cell. Proteomics MCP*. **13**, 2513–26 (2014).

43. S. Tyanova *et al.*, The Perseus computational platform for comprehensive analysis of (prote)omics data. *Nat. Methods*. **13**, 731–740 (2016).

## Acknowledgements

We thank Michael Bassik (Stanford) for the CRISPRi library and dCas9-KRAB expressing cell lines. We thank Thomas Waldmann (National Institutes of Health) for a gift of the HDLM-2 cell line. We thank Green Ahn (Stanford) for recombinant mCherry protein. We thank Eric Appel (Stanford) for use of aqueous gel permeation chromatography. This work was supported in part by National Institutes of Health grant P30CA124435 utilizing the Stanford Cancer Institute Proteomics/Mass Spectrometry Shared Resource. This work was supported in part by National Institutes of Health grant R01CA227942 to C.R.B. S.M.B was supported by a National Institute of General Medical Sciences F32 Postdoctoral Fellowship. K.P. was supported by a National Science Foundation Graduate Research Fellowship, a Stanford Graduate Fellowship, and the Stanford ChEM-H Chemistry/Biology Interface Predoctoral Training Program. S.W. was supported by a Banting Postdoctoral Fellowship from the Canadian Institutes of Health. N.M.R. was supported by National Institutes of Health grant K00CA21245403.

## Author contributions

S.M.B, K.P., and C.R.B. conceived the project. S.M.B., K.P., S.W., and N.M.R. carried out experiments and interpreted data. S.M.B and C.R.B. wrote the manuscript with input from all authors. C.R.B. provided supervision.

## Competing interests

A patent application relating to lysosome targeting chimeras has been filed by Stanford University (docket number STAN-1497PRV). C.R.B. is a co-founder and Scientific Advisory Board member of Palleon Pharmaceuticals, Enable Bioscience, Redwood Biosciences (a subsidiary of Catalent) and InterVenn Biosciences, and a member of the Board of Directors of Eli Lilly & Company.

## List of Supplementary materials

Materials and Methods
Fig. S1-S16
Supplemental Data 1
Supplemental Data 2

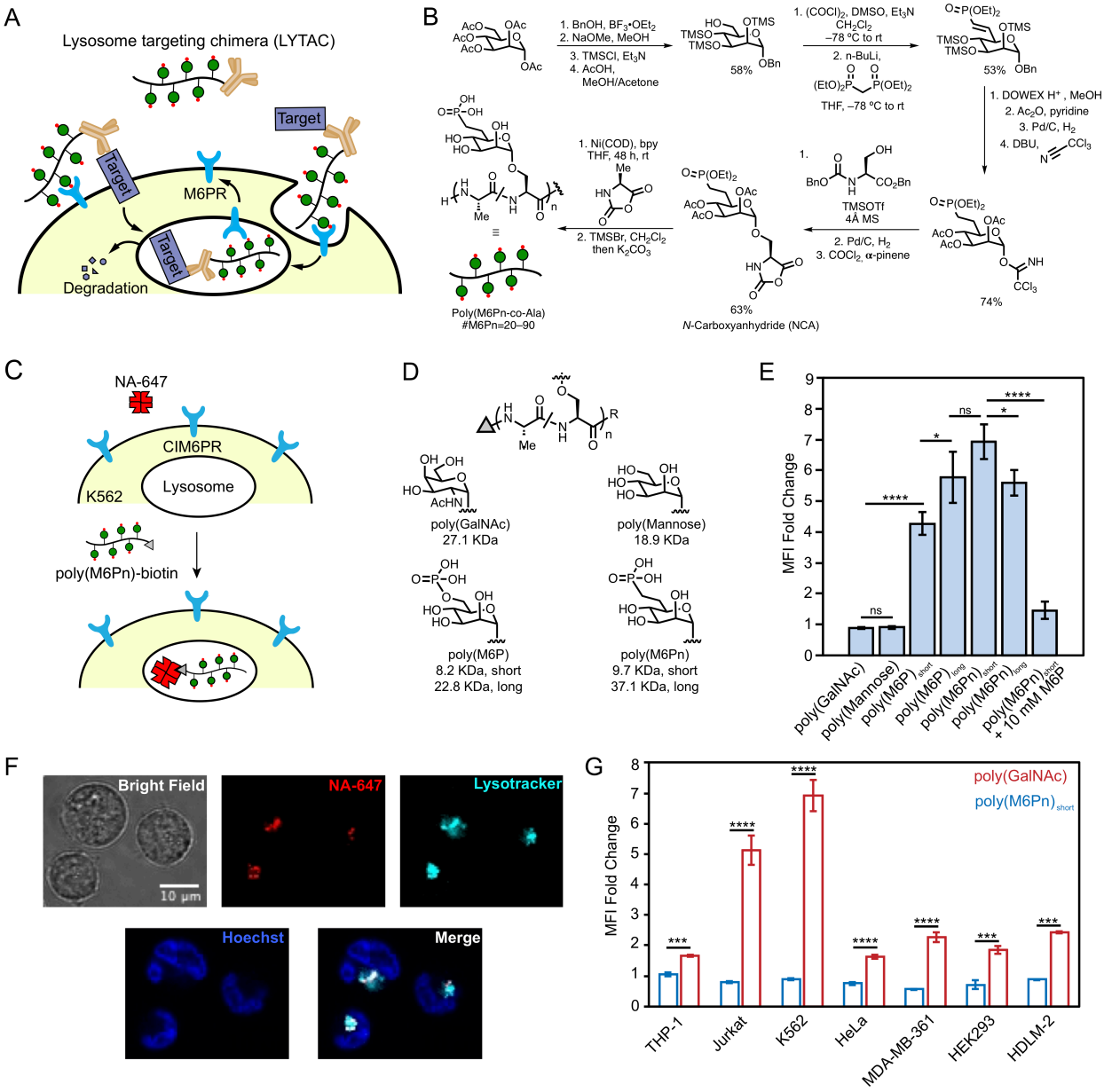


**Fig. 1. Lysosomal targeting chimeras (LYTACs) utilizing the cation-independent mannose-6-phosphate receptor (CI-M6PR) traffic proteins to lysosomes.** (A) LYTAC concept where a glycopolypeptide ligand for CI-M6PR is conjugated to an antibody to traffic secreted and membrane proteins to lysosomes. (B) Synthesis of mannose-6-phosphonate (M6Pn) glycopolypeptide agonists for CI-M6PR. (C) NeutrAvidin-647 (NA-647) internalization assay for biotin-based LYTACs. (D) Panel of synthetic M6P and M6Pn glycopolypeptides and controls. GalNAc = *N*-acetylgalactosamine. (E) Mean fluorescence intensity (MFI) fold changes for K562 cells incubated at 37 °C for 1 hour with 500 nM NA-647 or 500 nM NA-647 and 2 μM biotinylated glycopolypeptide in complete growth media. MFI determined by live cell flow cytometry and values are the average of three independent experiments ± SD. Fold change is relative to NA-647 uptake alone. (F) Live cell confocal microscopy images of K562 cells treated as in (E), then labeled with Lysotracker Green for 30 minutes. (G) Cell line panel for NA-647 uptake performed as in (E),

depicted values are the average of three independent experiments ± SD. *P < 0.05; **P < 0.01; ***P < 0.001; ****P < 0.0001, determined by Student's two-tailed t-test.

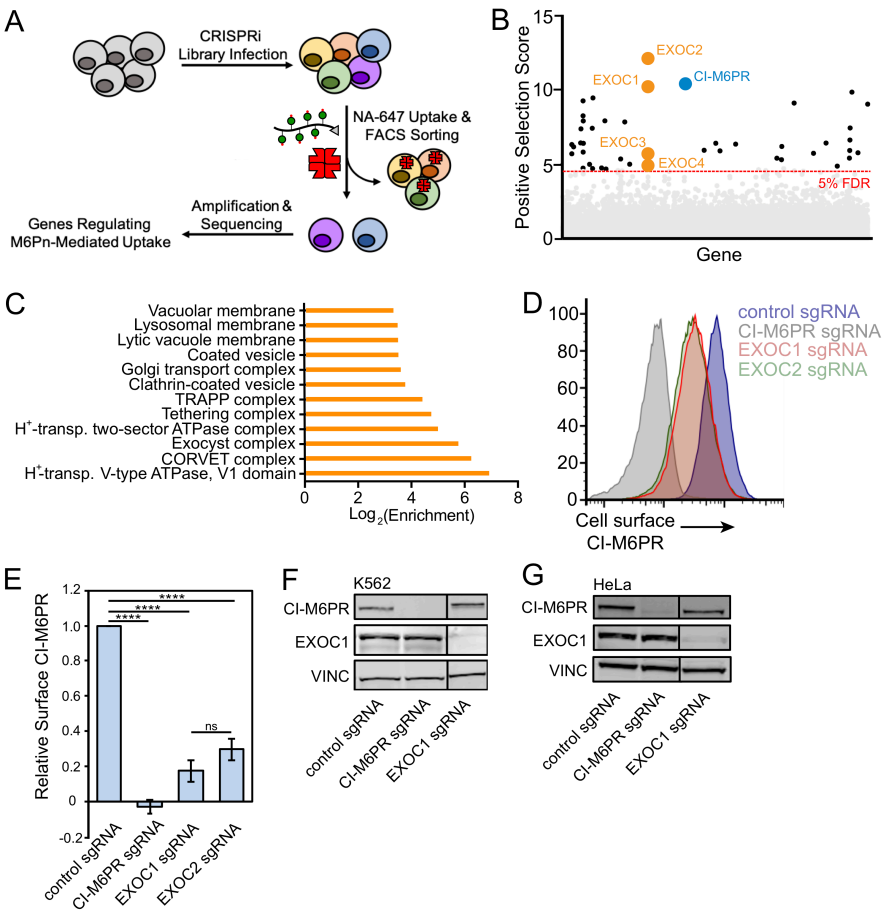


**Fig. 2. CRISPRi screen identifies key cellular machinery for LYTACs.** (A) CRISPRi screen in K562 cells stably expressing dCas9-KRAB and a library of sgRNAs with genome-wide coverage. (B) Gene hits for regulation of NA-647 internalization by LYTACs. (C) Gene ontology (GO) annotation for significant hits ( < 5% FDR). (D) and (E) Cell surface expression levels of CI-M6PR in dCas9-KRAB K562 cells (D) or HeLa cells (E) transfected with control sgRNA, CI-M6PR-targeting sgRNA, EXOC1-targeting sgRNA, or EXOC2-targeting sgRNA. Cells were stained for CI-M6PR and subjected to live cell flow cytometry. (D) is representative of two measurements for K562 cells, which rapidly lost the exocyst knockdown phenotype; (E) is the average of three independent experiments in HeLa ± SD and normalized to control sgRNA. *P < 0.05; **P < 0.01; ***P < 0.001; ****P < 0.0001, determined by Student's two-tailed t-test. (F) and (G) Western blot analysis of EXOC1 and CI-M6PR in K562 (F) and HeLa (G) CRISPRi knockdown lines.

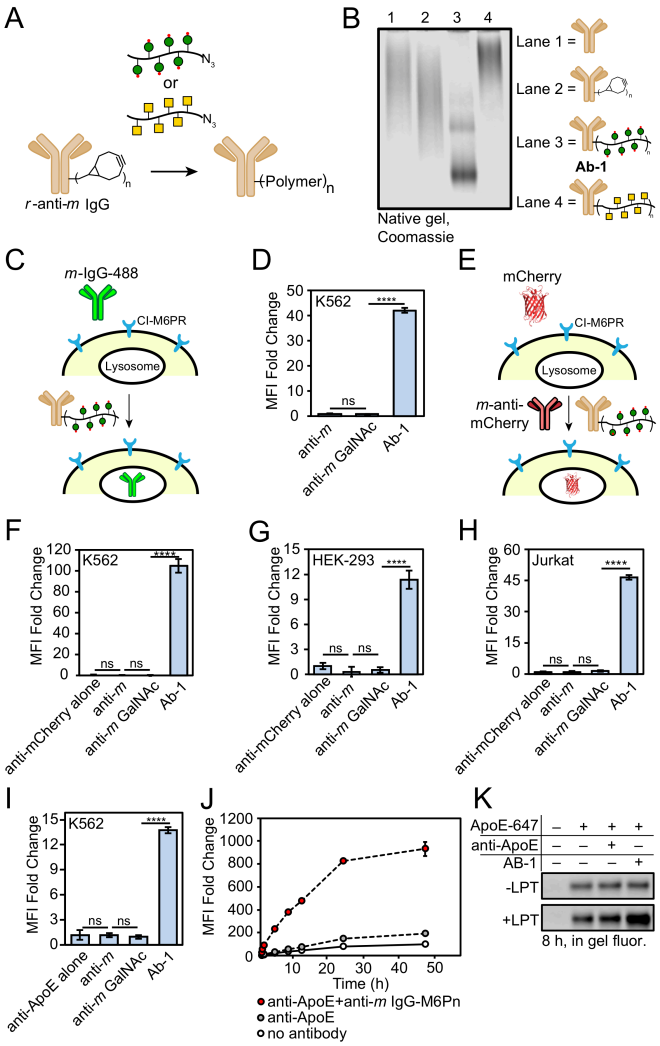


**Fig. 3. LYTACs target soluble proteins to lysosomes for degradation.** (A) Synthetic scheme for antibody-based LYTACs. (B) Native gel of polyclonal rabbit anti-mouse IgG conjugates. (C) Uptake of an AlexaFluor-488 labeled mouse IgG (m-IgG-488) into K562 cells using antibody LYTACs. (D) Mean fluorescence intensity fold change over background uptake measured by live cell flow cytometry. K562 cells were incubated at 37 °C for 1 hour with 50 nM IgG-488 or 50 nM IgG and 25 nM of anti-mouse or **Ab-1**. Values represent averages of three independent experiments ± SD. (E) Uptake of mCherry antigen and its antibody by a LYTAC into (F) K562 cells, (G) HEK-293 cells, or (H) Jurkat cells measured by live cell flow cytometry after 1 hour incubation as in (D). (I) Uptake of ApoE-647 into K562 cells, performed as in (D). Median fluorescence intensity was measured by live cell flow cytometry. Values represent averages of three independent experiments ± SD. (J) ApoE-647 uptake over time. K562 cells were incubated with 50 nM ApoE-647 in the presence or absence of anti-ApoE4 and **Ab-1**. At the indicated time point, cells were aliquoted and MFI measurements were taken as in (D). (K) Cells were incubated as in (D) for 8 hours in the presence or absence of 0.1 mg/mL leupeptin (LPT), then lysed. Lysates were separated by SDS-PAGE, and ApoE-647 was detected via in-gel fluorescence. *P < 0.05; **P < 0.01; ***P < 0.001; ****P < 0.0001, determined by Student's two-tailed t-test, fold changes are reported relative to incubation with protein targets alone.

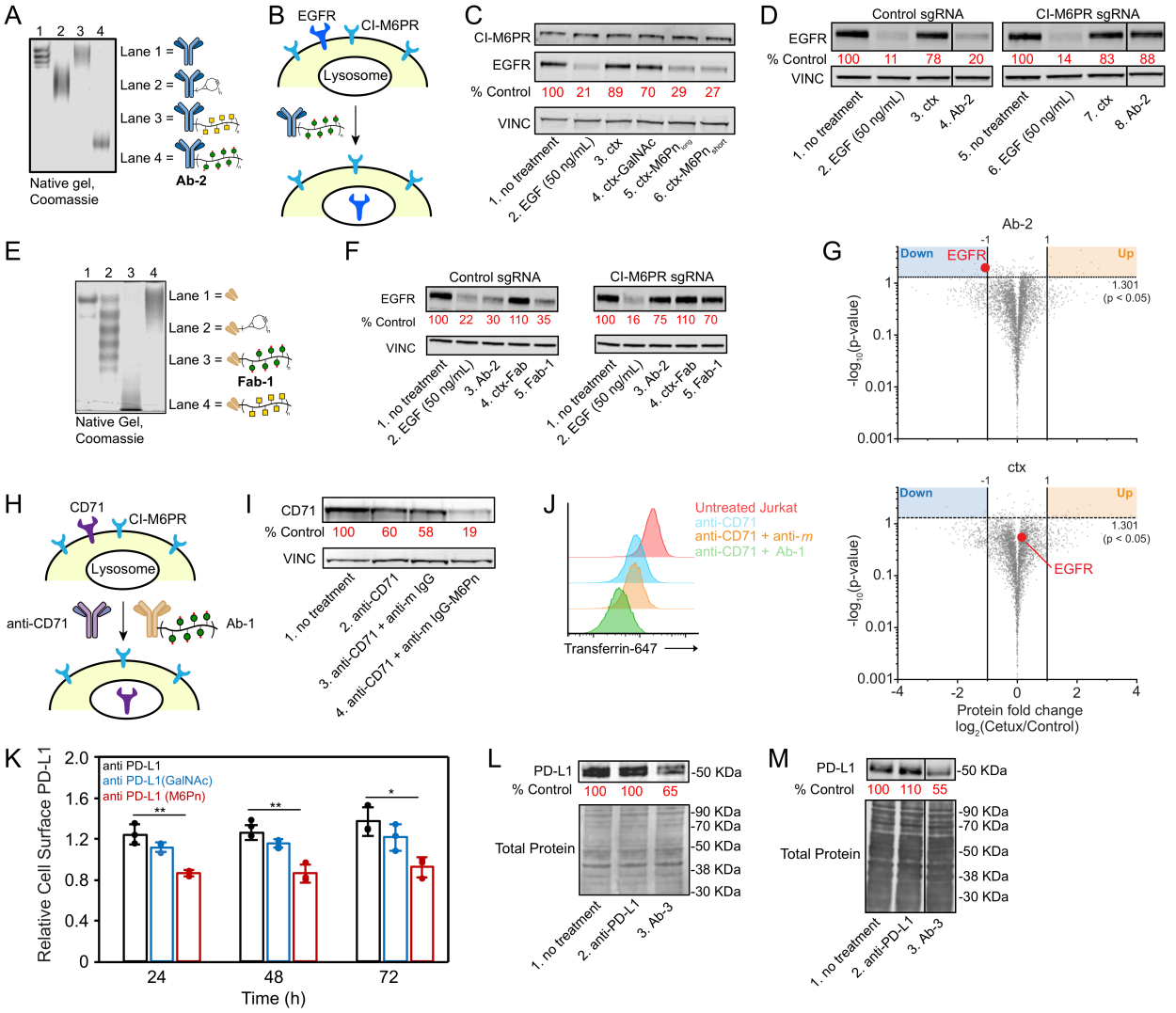


**Fig. 4. LYTACs accelerate degradation of membrane proteins.** (A) Native gel of cetuximab(ctx)-based LYTACs. (B) EGFR degradation using antibody LYTACs. (C) Western blot of HeLa cells treated with 100 nM ctx (lane 3), ctx-GalNAc (lane 4), ctx-M6Pn$_{long}$ (lane 5) or ctx-M6Pn$_{short}$ (lane 6) for 24 hours in complete growth media. EGF stimulation is a positive control for EGFR downregulation. (D) Western blot of EGFR degradation with 10 nM **Ab-2** for 24 hours in HeLa dCas9-KRAB cells expressing a control sgRNA or sgRNA targeting CI-M6PR. (E) Native gel of ctx-Fab-based LYTACs. (F) Western blot of EGFR degradation with **Fab-1** in HeLa dCas9-KRAB cells expressing a control sgRNA or sgRNA targeting CI-M6PR. (G) Fold change abundance of 3877 HeLa proteins detected via quantitative MS analysis following 24-hour treatment with either 10 nM **Ab-2** (top) or ctx (bottom). (H) Degradation of CD71 mediated by a primary antibody and **Ab-1**. (I) Western blot analysis of CD71 degradation in Jurkat cells after 24 hours. (J) Uptake of transferrin-647 in Jurkat cells treated with anti-CD71 or anti-CD71 and **Ab-1** for 24 hours. (K) Cell surface PD-L1 determined by live cell flow cytometry after incubation with anti-PD-L1 or conjugates (50 nM). At each time point, cells were lifted, brought to 4 °C, then stained for PD-L1. Cell surface PD-L1 is reported relative to untreated and PD-L1 stained cells. (L) and (M) Western blot analysis of total PD-L1 in MDA-MB-231 after 48 hours (L) and HDLM-2 after 36 hours (M). Percent control values were calculated via densitometry and normalized to

loading control or total protein. *P < 0.05; **P < 0.01; ***P < 0.001; ****P < 0.0001, determined by Student's two-tailed t-test.

# Supplementary Materials for

**Lysosome Targeting Chimeras (LYTACs) for the Degradation of Secreted and Membrane Proteins**

Steven M. Banik, Kayvon Pedram, Simon Wisnovsky, Nicholas M. Riley, Carolyn R. Bertozzi*

*Correspondence should be addressed to C.R.B. (bertozzi@stanford.edu).

**This PDF file includes:**

Materials and Methods
Fig. S1-S16

**Other Supplementary Materials for this manuscript include the following:**

Supplemental Data 1
Supplemental Data 2

## Materials and Methods

**General Synthetic Chemistry Procedures and Materials:** All reactions were performed in standard, dry glassware fitted with rubber septa under an inert atmosphere of nitrogen unless otherwise described. Stainless steel syringes or cannulae were used to transfer air- and moisture-sensitive liquids. Reported concentrations refer to solution volumes at room temperature. Column chromatography was performed with ZEOprep® 60 (40–63 micron) silica gel from American Scientific. Thin layer chromatography (TLC) was used for reaction monitoring and product detection using pre-coated glass plates covered with 0.20 mm silica gel with fluorescent indicator; visualization by UV light, $KMnO_4$, or 5% $H_2SO_4$ in MeOH. Reagents were purchased in reagent grade from commercial suppliers and used as received, unless otherwise described. Anhydrous solvents (acetonitrile, benzene, dichloromethane, diethyl ether, *N*,*N*-dimethylformamide, tetrahydrofuran, and toluene) were prepared by passing the solvent through an activated alumina column.

**Chemical Analysis Instrumentation:** Proton nuclear magnetic resonance ($^1$H NMR) spectra were recorded on an Inova-600 spectrometer or a Varian-400 spectrometer at 25 °C, are reported in parts per million downfield from tetramethylsilane, and are referenced to the residual protium resonances of the NMR solvent ($CDCl_3$: 7.26 [$CHCl_3$], $CD_3OD$: 4.87 [MeOH], $D_2O$: 3.31 [$H_2O$]). Proton-decoupled carbon-13 nuclear magnetic resonance ($^{13}$C {$^1$H} NMR) spectra were recorded on an Varian-400 spectrometer at 25 °C, are reported in parts per million downfield from tetramethylsilane, and are referenced to the carbon resonances of the NMR solvent ($CDCl_3$: 77.16, $CD_3OD$: 49.00). Chemical shifts for phosphorus-31 nuclear magnetic resonance ($^{31}$P NMR) were recorded on a Varian Mercury-400 spectrometer at 25 °C, are reported in parts per million downfield from $H_3PO_4$ (δ = 0). Data are represented as follows: chemical shift, multiplicity (br = broad, s = singlet, d = doublet, t = triplet, q = quartet, quin = quintet, sept = septet, m = multiplet), coupling constants in Hertz (Hz), integration. High-resolution mass spectrometric data were obtained on a Thermo Exactive benchtop Orbitrap.

### Synthesis of Mannose-6-Phosphonate *N*-Carboxyanhydride Monomers:

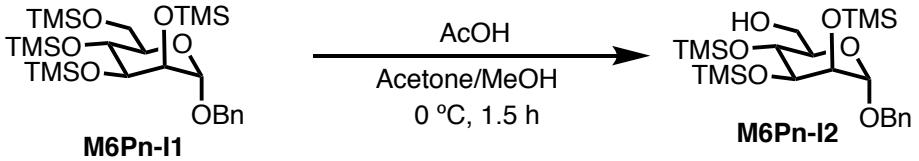


**M6Pn-I2.** To **M6Pn-I1** (*33*) (5.65 g, 10.1 mmol, 1.0 equiv.) was added acetone (22 mL) and methanol (30 mL). The mixture was cooled to 0 °C, and acetic acid (1.11 mL) was added. The reaction was stirred for 1.5 hours at 0 °C, after which solid $NaHCO_3$ (1.79 g, 21.3 mmol, 2.10 equiv.) was added. The reaction mixture was concentrated under reduced pressure and the resulting residue was purified by flash column chromatography on silica gel (0 to 15% ethyl acetate in hexanes) to give a colorless oil (2.80 g, 58%). $^1$H NMR (400 MHz, $CDCl_3$) δ 7.38–7.28 (m, 5H), 4.73–4.70 (d, *J* = 12.2 Hz, 1H), 4.69 (s, 1H), 4.51–4.48 (d, *J* = 12.2 Hz, 1H), 3.92–3.59 (m, 6H), 2.01 (s, 1H), 0.17 (s, 9H), 0.16 (s, 9H), 0.12 (s, 9H). $^{13}$C NMR (101 MHz, $CDCl_3$) δ 137.6, 128.4, 127.7, 127.6, 100.3, 74.1, 73.7, 72.5, 69.0, 68.1, 62.2, 0.66, 0.58, 0.35. ESI-HRMS Calc'd [M+$NH_4^+$]=504.2633; found 504.2627.

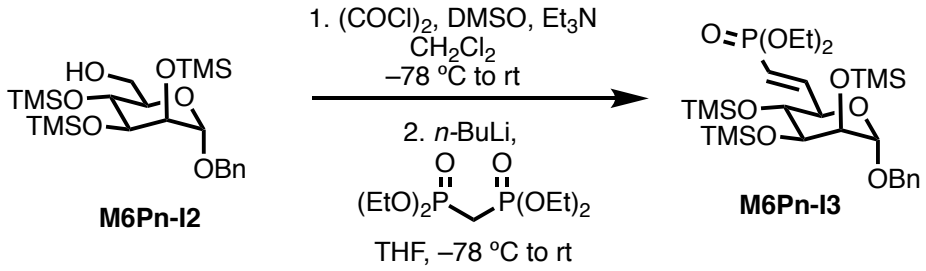


**M6Pn-I3.** To oxalyl chloride (0.649 mL, 5.87 mmol, 1.1 equiv.) was added dichloromethane (10 mL), and the mixture was cooled to -78 °C. To the reaction mixture was added DMSO (0.834 mL, 11.74 mmol, 2.2 equiv.), and the reaction was stirred for 10 minutes at -78 °C. To the reaction mixture was added a solution of **M6Pn-I2** (2.60 g, 5.34 mmol, 1.0 equiv.) in dichloromethane (10 mL) dropwise, and the reaction was stirred at -78 °C. After 45 minutes, triethylamine (3.72 mL, 26.7 mmol, 5.0 equiv) was added, and the mixture was allowed to warm to room temperature and stirred for 1 hour. The reaction mixture was diluted with dichloromethane (150 mL) and washed with water (3 X 50 mL). The organic layer was dried with $MgSO_4$ and concentrated under reduced pressure to give an orange residue. To tetraethyl methylenediphosphonate (2.31 g, 8.01 mmol, 1.5 equiv.) was added tetrahydrofuran (30 mL) and the reaction mixture was cooled to –78 °C. To the reaction mixture was added *n*-BuLi (2.5 M in hexanes, 2.67 mL, 6.67 mmol, 1.25 equiv.). After 45 minutes, the orange residue obtained above was added slowly as a solution in tetrahydrofuran (10 mL), and the reaction mixture was stirred at -78 °C for two hours, then allowed to warm to room temperature overnight. The reaction mixture was diluted with ethyl acetate (250 mL) and washed with water (2 X 50 mL). The organic layer was dried with $MgSO_4$ and concentrated under reduced pressure. The resulting residue was purified by flash column chromatography on silica gel (0 to 40% ethyl acetate in hexanes) to give a colorless oil (1.93 g, 53% over two steps). $^1$H NMR (400 MHz, $CDCl_3$) δ 7.44–7.21 (m, 5H), 6.85 (ddd, *J* = 22.8, 17.2, 4.2 Hz, 1H), 6.05 (ddd, *J* = 22.0, 17.2, 1.8 Hz, 1H), 4.70 (m, 1H), 4.67–4.45 (d, *J* = 12.2 Hz, 1H), 4.48–4.45 (d, *J* = 12.2 Hz, 1H), 4.14 – 4.05 (m, 6H), 3.83 – 3.80 (m, 2H), 3.69 ( app. t, *J* = 9.6 Hz, 2H), 1.33 (td, *J* = 7.1, 1.3 Hz, 4H), 0.16 (s, 9H), 0.13 (s, 9H), 0.10 (s, 9H). $^{13}$C NMR (101 MHz, $CDCl_3$) δ 148.9 (d, J = 5.9 Hz), 137.5, 128.4, 127.7, 127.6, 117.0 (d, *J* = 189.2 Hz), 100.2, 73.5, 73.3, 72.8, 71.5, 69.1, 61.6 (t, *J* = 6.1 Hz), 16.4 (d, *J* = 6.2 Hz), 0.74, 0.56, 0.32. $^{31}$P NMR (162 MHz, $CDCl_3$) δ 18.5. ESI-HRMS Calc'd [M+H$^+$, -3 X TMS]=403.1522; found 403.1514.

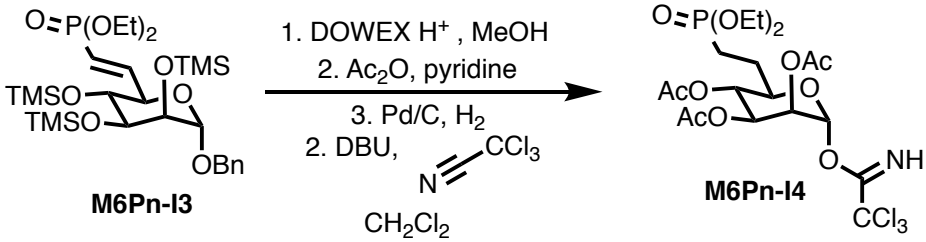


**M6Pn-I4.** To **M6Pn-I3** (1.93 g, 3.12 mmol, 1.0 equiv) was added methanol (40 mL) and DOWEX 50 WX8-200 (1.0 g). The mixture was stirred for 1 hour at room temperature. The reaction mixture was filtered and concentrated under reduced pressure. The resulting residue was dissolved in pyridine (20 mL), and acetic anhydride (10 mL) was added. The reaction was allowed to stir overnight, then concentrated under reduced pressure. The residue was dissolved in dichloromethane (100 mL) and washed with 1M HCl (50 mL) and water (50 mL). The organic layer was dried with anhydrous $MgSO_4$ and concentrated under reduced pressure. To the

resulting residue was added 10% Pd/C (666 mg, 0.624 mmol, 0.2 equiv.), and methanol (40 mL), and the reaction mixture was degassed and placed under an atmosphere of hydrogen. After 24 hours, additional Pd/C was added (2.00 g), and the reaction was stirred under an atmosphere of hydrogen for an additional 24 hours. Upon completion, the reaction mixture was filtered through celite and concentrated. To the resulting residue was added dichloromethane (50 mL), trichloroacetonitrile (3.12 mL, 31.2 mmol, 10.0 equiv.), and DBU (0.046 mL, 0.0312 mmol, 0.1 equiv.). The reaction mixture was allowed to stir for 1 hour at room temperature, then concentrated under reduced pressure. The resulting residue was purified by flash column chromatography on silica gel (30 to 100% ethyl acetate in hexanes) to give a pale yellow foam (1.35 g, 74% over 4 steps). $^{1}$H NMR (400 MHz, $CDCl_3$) δ 8.70 (s, 1H), 6.09 (s, 1H), 5.33–5.31 (m, 1H), 5.22 (dd, *J* = 10.0, 3.4 Hz, 1H), 5.07 (app. t, *J* = 10.0 Hz, 1H), 4.00–3.88 (m, 4H), 3.82 (app. t, *J* = 8.1 Hz, 1H), 2.06 (s, 3H), 1.95 (s, 3H), 1.87 (s, 3H), 1.82–1.43 (m, 4H), 1.18 (t, *J* = 7.1 Hz, 6H). $^{13}$C NMR (101 MHz, $CDCl_3$) δ 169.6, 169.5, 169.5, 159.5, 94.2, 90.4, 72.2 (d, *J* = 18.0 Hz), 68.7, 67.9 (d, *J* = 16.8 Hz), 61.5 (d, *J* = 6.9 Hz), 61.4 (d, *J* = 7.0 Hz), 24.1 (d, *J* = 4.0 Hz), 21.6, 20.6, 20.6, 20.5, 20.1, 16.4 (d, *J* = 5.9 Hz). $^{31}$P NMR (162 MHz, $CDCl_3$) δ 31.2. ESI-HRMS Calc'd $[M+H^+]$=584.0622; found 584.0607.

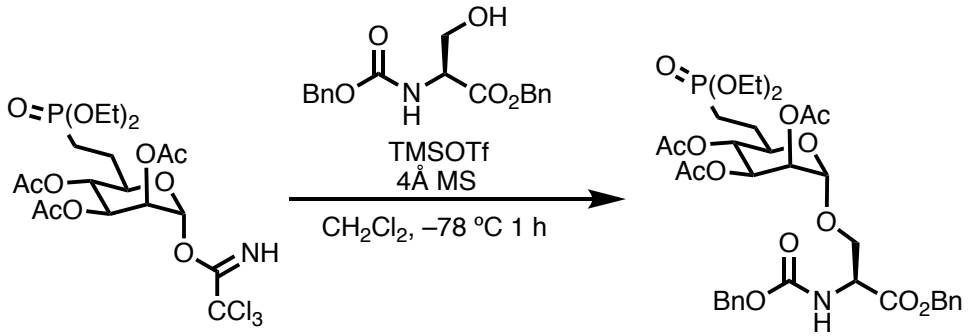


**M6Pn-I4** **M6Pn-I5**

**M6Pn-I5.** To **M6Pn-I4** (1 g, 1.71 mmol, 1.25 equiv.) was added Z-Ser-OBn (451 mg, 1.37 mmol, 1.0 equiv.), 3 g freshly activated 4Å MS, and dichloromethane (50 mL). The reaction mixture was cooled to -78 °C and TMSOTf (0.060 mL, 0.342 mmol, 0.2 equiv.) was added and the reaction mixture was stirred at -78 °C for 1 h. Triethylamine (1 mL) was added to reaction mixture, and the resulting mixture was filtered over celite and concentrated. The resulting residue was purified by flash column chromatography on silica gel (30 to 100% ethyl acetate in hexanes) to give a white foam (1.02 g, 79%). $^{1}$H NMR (400 MHz, $CDCl_3$) δ 7.34–7.28 (m, 10H), 5.84 (d, *J* = 8.0 Hz, 1H), 5.31 – 4.95 (m, 8H), 4.63 (s, 1H), 4.55 (d, *J* = 7.7 Hz, 2H), 4.09–3.95 (m, 4H), 3.92–3.90 (m, 2H), 3.72–3.68 (m, 1H), 2.10 (s, 3H), 2.00 (s, 3H), 1.95 (s, 3H), 1.84–1.66 (m, 4H), 1.27 (t, *J* = 7.1 Hz, 6H). $^{13}$C NMR (101 MHz, $CDCl_3$) δ 169.7, 169.6, 169.3, 155.8, 136.0, 135.0, 128.5, 128.4, 128.4, 128.3, 128.1, 128.0, 97.7, 69.8 (d, *J* = 17.2 Hz), 68.5 (d, *J* = 40.4 Hz), 67.5, 67.1, 61.5 (d, *J* = 4.6 Hz), 61.5 (d, *J* = 5.4 Hz), 54.2, 24.1 (d, *J* = 4.1 Hz), 20.8 (d, *J* = 143.3 Hz), 20.6, 20.6, 20.5, 20.1, 16.3 (d, *J* = 6.0 Hz). $^{31}$P NMR (162 MHz, $CDCl_3$) δ 31.3. ESI-HRMS Calc'd $[M+H^+]$=752.2683; found 752.2670.

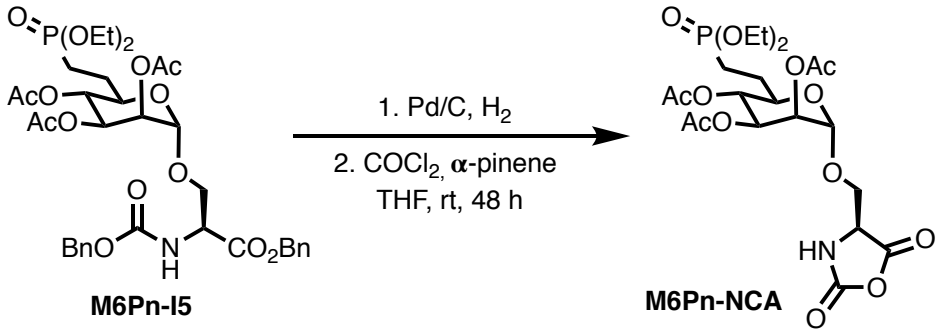


**M6Pn-NCA.** To **M6Pn-I5** (500 mg, 0.665 mmol, 1.0 equiv.) was added 10% Pd/C (71 mg, 0.067 mmol, 0.1 equiv.), and methanol (15 mL), and the reaction mixture was degassed and placed under an atmosphere of hydrogen. After 12 hours, the reaction mixture was filtered over celite and concentrated to give the corresponding amino acid. The resulting residue was dissolved in tetrahydrofuran (15 mL), and α-pinene (422 µL, 2.66 mmol, 4.00 equiv), and phosgene (950 µL, 1.33 mmol, 2.00 equiv.) were added. The reaction mixture was allowed to stir for 48 hours, then concentrated under reduced pressure into a cold trap in a fumehood. The resulting tan residue was purified by flash column chromatography on anhydrous silica gel (0 to 30% anhydrous tetrahydrofuran in anhydrous dichloromethane) to give a white foam (420 mg, 80%). $^{1}$H NMR (400 MHz, $CDCl_3$) δ 8.76 – 8.73 (m, 1H), 5.24 (dd, *J* = 3.4, 1.8 Hz, 1H), 5.11 (dd, *J* = 10.1, 3.4 Hz, 1H), 5.02 (app. t, *J* = 9.9 Hz, 1H), 4.79 (d, *J* = 1.8 Hz, 1H), 4.36 (app. t, *J* = 2.3 Hz, 1H), 4.25–3.96 (m, 6H), 3.85 (dd, *J* = 9.6, 2.2 Hz, 1H), 2.11 (s, 3H), 2.05 (s, 3H), 1.94 (s, 3H), 1.92–1.60 (m, 4H), 1.35 (t, *J* = 7.0 Hz, 3H), 1.31 (t, *J* = 7.1 Hz, 3H). $^{13}$C NMR (101 MHz, $CDCl_3$) δ 170.2, 169.9, 169.3, 168.9, 152.2, 96.8, 69.9, 69.3, 68.7, 68.5 (d, *J* = 2.6 Hz), 64.2, 62.5 (d, *J* = 7.0 Hz), 62.1 (d, *J* = 6.7 Hz), 58.1, 25.3 (d, *J* = 5.7 Hz), 20.9, 20.9, 20.7, 20.3 (d, *J* = 143.1 Hz), 16.6 (d, *J* = 5.9 Hz), 16.5 (d, *J* = 6.1 Hz) $^{31}$P NMR (162 MHz, $CDCl_3$) δ 29.4. ESI-HRMS Calc'd [M+H$^+$]=554.1639; found 554.1627.

**Synthesis of Mannose-6-Phosphate *N*-Carboxyanhydride Monomers:**

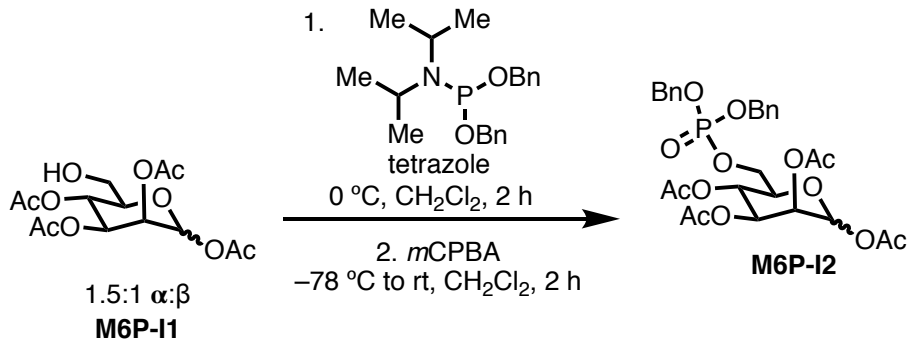


**M6P-I2.** To **M6P-I1** (*34*) (5.00 g, 14.4 mmol, 1.00 equiv.) was added 1*H*-tetrazole (2.03 g, 28.8 mmol, 2.00 equiv.) and dichloromethane (288 mL). The mixture was cooled to 0 °C, and dibenzyl *N,N*-diisopropylphosphoramidite (7.26 mL, 21.6 mmol, 1.5 equiv.) was added dropwise over 5 minutes. After 2 hours, the reaction mixture was cooled to -78 °C, and *m*CPBA (12.91 g of 77% *m*CPBA, 57.6 mmol, 4 equiv.) was added as a solid. The reaction was allowed to warm to 0 °C. After two hours, saturated $Na_2S_2O_3$ (100 mL) was added, and the organic layer was removed, washed 2X with saturated $NaHCO_3$ (150 mL), dried with $MgSO_4$, and concentrated under reduced pressure. The resulting residue was purified by flash column chromatography on silica gel (10 to 90% ethyl acetate in hexanes) to give a colorless, viscous oil (8.01 g, 91%). $^{1}$H NMR (400 MHz,

$CDCl_3$, two diastereomers) 7.31–7.23 (m, 10H), 6.25 (d, *J* = 3.7 Hz, 1H), 5.66 (d, *J* = 8.3 Hz, 1H), 5.39 (t, *J* = 9.9 Hz, 1H), 5.18 (t, *J* = 9.4 Hz, 1H), 5.09 – 4.90 (m, 8H), 4.16 – 3.93 (m, 3H), 3.73 (dd, *J* = 9.9, 1.6 Hz, 1H), 2.06 (s, 3H), 1.97 (s, 3H), 1.96 (s, 3H), 1.95 (s, 6H), 1.93 (s, 3H), 1.92 (s, 3H). $^{13}C$ NMR (101 MHz, $CDCl_3$) δ 170.1, 170.0, 169.5, 169.2, 169.1, 168.7, 168.6, 135.7, 135.6, 128.5, 128.5, 127.9, 127.9, 127.8, 91.5, 88.8, 73.0 (d, *J* = 8.1 Hz), 72.7, 70.2 (d, *J* = 8.1 Hz), 70.1, 69.7, 69.4 (d, *J* = 1.6 Hz), 69.4, 69.0, 67.7, 67.6, 65.0 (d, *J* = 5.2 Hz), 64.9 (d, *J* = 5.8 Hz), 20.7, 20.6, 20.5, 20.4, 20.3. $^{31}P$ NMR (162 MHz, $CDCl_3$) δ -1.3, -1.5. ESI-HRMS Calc'd $[M+H^+]$=609.1737; found 609.1728.

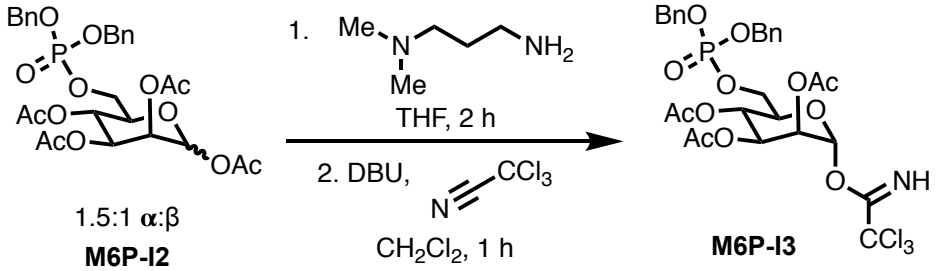


**M6P-I3.** To **M6P-I2** (8.01 g, 13.2 mmol, 1.00 equiv.) was added tetrahydrofuran (66 mL), followed by 3-(dimethylamino)-1-propylamine (4.15 mL, 33.0 mmol, 2.5 equiv.). The reaction was allowed to stir 1.5 hours until complete consumption of the starting material was observed. The reaction mixture was diluted with dichloromethane (250 mL) and washed with 1M HCl (100 mL) and water (100 mL). The organic layer was dried with $MgSO_4$ and concentrated under reduced pressure. To the resulting residue was added dichloromethane (250 mL), trichloroacetonitrile (6.62 mL, 66.0 mmol, 5.0 equiv.), and DBU (0.197 mL, 1.32 mmol, 0.1 equiv.). The reaction mixture was allowed to stir for 1 hour at room temperature, then concentrated under reduced pressure. The resulting residue was purified by flash column chromatography on silica gel (10 to 85% ethyl acetate) to give a pale yellow, viscous oil (6.10g, 65% over two steps). $^1H$ NMR (400 MHz, $CDCl_3$) δ 8.70 (s, 1H), 6.20 (s, 1H), 5.38 (s, 1H), 5.36 – 5.27 (m, 2H), 4.97 (app. t, *J* = 6.8 Hz, 4H), 4.25 – 3.89 (m, 3H), 2.02 (s, 3H), 1.96 (s, 3H), 1.94 (d, *J* = 6.8 Hz, 3H). $^{13}C$ NMR (101 MHz, $CDCl_3$) δ 169.7, 169.6, 169.4, 159.4, 135.7 (d, *J* = 4.1 Hz), 135.6 (d, *J* = 4.1 Hz), 128.5, 128.4, 127.9, 127.8, 94.3, 71.7 (d, *J* = 7.8 Hz), 69.4 (d, *J* = 2.2 Hz), 69.3 (d, *J* = 2.1 Hz), 68.7, 67.7, 65.4 (d, *J* = 5.2 Hz), 65.1, 20.6, 20.6, 20.6. $^{31}P$ NMR (162 MHz, $CDCl_3$) δ -1.35. ESI-HRMS Calc'd $[M+H^+]$=710.0728; found 710.0714.

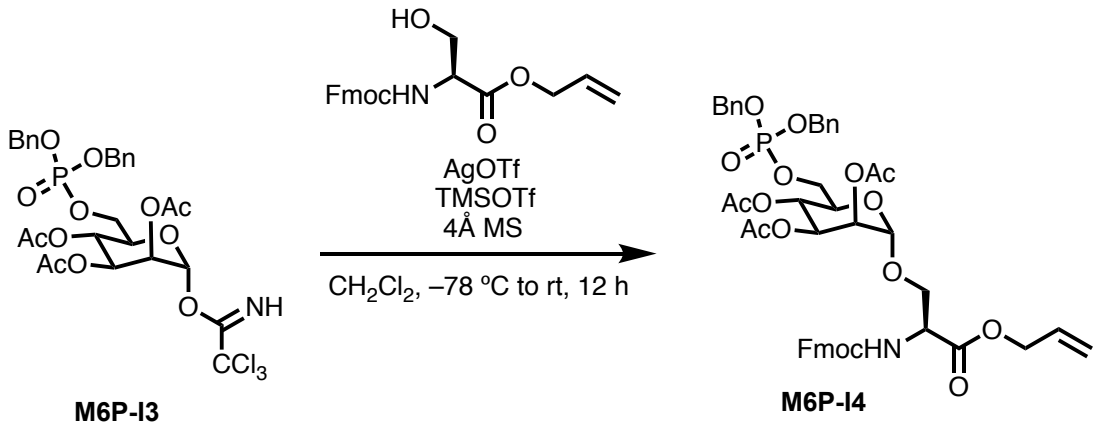

**M6P-I4.** To **M6P-I3** (4.00 g, 5.63 mmol, 1.0 equiv.) was added Fmoc-Ser allyl ester (2.48 g, 6.76 mmol, 1.2 equiv.), AgOTf (2.89 g, 11.26 mmol, 2.0 equiv.), freshly activated 4Å MS (12.0 g), and dichloromethane (320 mL). The reaction mixture was cooled to -78 °C and TMSOTf (0.255 mL, 1.41 mmol, 0.25 equiv.) was added. The reaction was allowed to warm to -40 °C, stirred at that temperature for 1 h, then allowed to warm to room temperature over 12 hours. Triethylamine (1.0 mL) was added to reaction mixture, and the resulting mixture was filtered over celite and concentrated. The resulting residue was purified by flash column chromatography on silica gel (10 to 100% ethyl acetate in hexanes) to give a white foam (2.33g, 45%). ESI-HRMS Calc'd $[M+H^+]$=916.2945; found 916.2925.

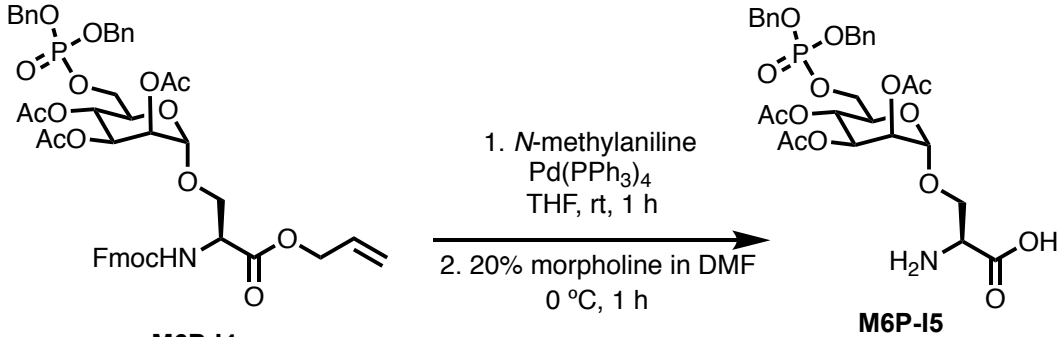


**M6P-I4** **M6P-I5**

**M6P-I5.** To **M6P-I4** (2.33 g, 2.54 mmol, 1.0 equiv.) was added tetrahydrofuran (109 mL), $Pd(PPh_3)_4$ ( 210 mg, 0.181 mmol, 0.071 equiv.), and *N*-methylaniline (2.75 mL, 25.4 mmol, 10.0 equiv.). The reaction mixture was stirred for 1 hour at room temperature, then concentrated under reduced pressure. The resulting residue was purified by flash column chromatography on silica gel (20 to 100% ethyl acetate in hexanes) to give a light brown foam, which was dissolved in *N*,*N*-dimethylformamide (48.0 mL) and cooled to 0 °C. Morpholine (12.0 mL) was added, and the reaction was stirred at 0 °C for 1 hour. The reaction mixture was concentrated under reduced pressure and purified by flash column chromatography on silica gel (100% ethyl acetate to 33% MeOH in ethyl acetate to 33% MeOH in ethyl acetate with 17% $H_2O$) to give a tan foam (743 mg, 45% over two steps). $^1$H NMR (400 MHz, $CD_3OD$) δ 7.55 – 7.11 (m, 10H), 5.39–5.34 (m, 1H), 5.31 (s, 1H), 5.30–5.28 (m, 1H), 5.10–5.00 (m, 4H), 4.20–4.14 (m, 2H), 4.11–4.04 (m, 2H), 3.81–3.71 (m, 2H), 1.96 (s, 3H), 1.95 (s, 3H), 1.92 (s, 3H). $^{13}$C NMR (101 MHz, $CD_3OD$) δ 171.8, 171.4, 171.2, 137.2 (m), 129.8 (d, *J* = 1.2 Hz), 129.7, 129.2, 129.2, 99.5, 71.0, 70.9, 70.9, 70.8, 70.5 (d, *J* = 7.8 Hz), 70.2, 68.2, 66.9 (d, *J* = 5.3 Hz), 66.5, 55.0, 20.7, 20.6, 20.6. $^{31}$P NMR (162 MHz, $CD_3OD$) δ -1.87. ESI-HRMS Calc'd $[M+H^+]$=654.1952; found 654.1941.

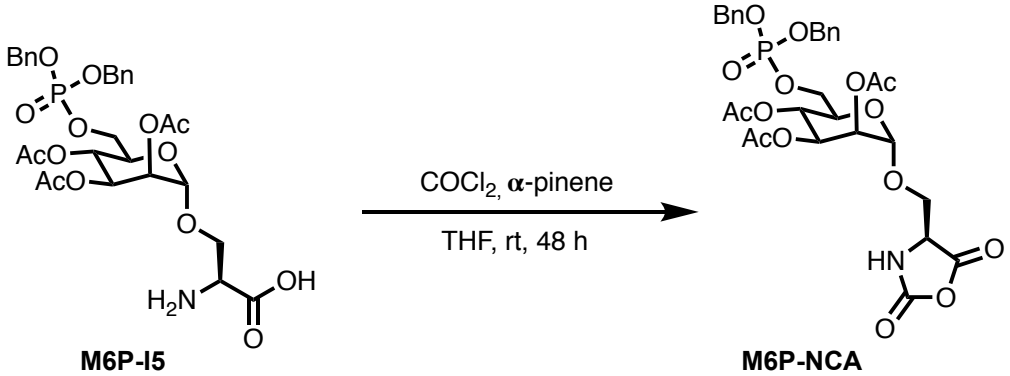


**M6P-I5** **M6P-NCA**

**M6P-NCA.** To **M6P-I5** (350 mg, 0.536 mmol, 1.0 equiv.) was added 12 mL tetrahydrofuran, α-pinene (340 µL, 2.14 mmol, 4.00 equiv.), and phosgene (765 µL, 1.07 mmol, 2.00 equiv.). The reaction mixture was allowed to stir for 48 hours, then concentrated under reduced pressure into a cold trap in a fumehood. The resulting tan residue was purified by flash column chromatography on anhydrous silica gel (0 to 30% anhydrous tetrahydrofuran in anhydrous dichloromethane) to give a white foam (290 mg, 80%). $^{1}$H NMR (400 MHz, $CDCl_3$) δ 8.19 (s, 1H), 7.40–7.25 (m, 10H), 5.25 (dd, *J* = 3.5, 1.8 Hz, 1H), 5.17–4.95 (m, 6H), 4.80 (s, 1H), 4.33–4.30 (m, 1H), 4.25–4.18 (m, 1H), 4.11–3.95 (m, 3H), 3.82 (dd, *J* = 10.1, 2.8 Hz, 1H), 2.09 (s, 3H), 1.95 (s, 3H), 1.88 (s, 3H). $^{13}$C NMR (101 MHz, $CDCl_3$) 170.3, 169.8, 169.4, 168.3, 152.1, 135.4 (d, *J* = 6.7 Hz), 135.3 (d, *J* = 6.9 Hz), 129.0, 129.0, 128.9, 128.8, 128.3, 128.0, 97.1, 70.2 (d, *J* = 1.0 Hz), 70.12 (d, *J* = 1.9 Hz), 69.5 (d, *J* = 1.8 Hz), 69.0, 68.5, 67.70 (d, *J* = 6.3 Hz), 66.6, 64.7, 58.0, 20.8, 20.7, 20.6. δ $^{31}$P NMR (162 MHz, $CDCl_3$) δ -3.18. ESI-HRMS Calc'd [$M+H^+$]=680.1744; found 680.1735.

**General Procedure for M6Pn/M6P-containing Glycopolypeptide Synthesis:** Polymerization is performed in a glovebox under a $N_2$ atmosphere. The polymerization catalyst was prepared fresh following the procedure of Kramer *et al*. (*20*), using Ni(COD) and 2,2'-bipyridyl. To an oven dried 1-mL vial was added 20 mg M6Pn-NCA, 4.2 mg Alanine NCA, and 161 µL freshly prepared catalyst mixture (stoichiometry relative to initiator = 5:5:1). The reaction mixture turned from deep purple to red, and was incubated for 48 hours at ambient temperature in the glovebox. After 48 hours, the vial was removed from the glovebox and the reaction mixture quenched with acidic methanol and evaporated under reduced pressure. For both M6Pn and M6P containing polymerization reactions, reactions proceeded slowly without alanine-NCA used as a comonomer, while reaction completion of 1:1 mixtures was obtained within 48 hours.

**General Procedure for M6Pn-Containing Polymer Deprotection:** To the resulting residue obtained above was added 1 mL anhydrous DCM, 50 µL TMSBr (10 equiv. per phosphonate group), and 30 µL pyridine (10 equiv. per phosphonate). The reaction mixture was stirred at room temperature overnight sealed under $N_2$. After concentrating under vacuum, the reaction mixture was suspended in a 1:1:1 mixture of 2 mL MeOH with 2 mL THF and 2 mL saturated aqueous $K_2CO_3$. After 48 hours, 2 mL $H_2O$ was added, in which some of the precipitate dissolved to yield a cloudy solution that was further stirred for 24 hours. The reaction mixture was neutralized to pH = 7 using concentrated HCl, and evaporated to dryness under reduced pressure. The resulting residues and salts were dissolved in $H_2O$ and dialyzed in a 3.5 KDa MWCO dialysis cassette against $H_2O$ for 3 days, with $H_2O$ changes every 8 hours for the first 24 hours, followed by every 12 hours subsequently. The dialysate was removed from the cassette and any precipitate was removed by filtration through a 0.2 µM filter. The resulting solution was lyophilized to yield white solids.

**General Procedure for M6P-Containing Polymer Deprotection:** To the residue obtained above was added Pd/C (100 mol% Pd per phosphate group) and a dichloromethane/methanol mixture (1:1, 2 mL total/20 mg NCA used in polymerization), and the reaction was stirred under a balloon of $H_2$ for 48 hours. After filtration through a 0.2 µM filter, the resulting residue was concentrated under vacuum and resuspended in a 1:1:1 mixture of 2 mL MeOH with 2 mL THF and 2 mL saturated aqueous $K_2CO_3$. After 48 hours, 2 mL $H_2O$ was added, in which some of the precipitate dissolved to yield a cloudy solution that was further stirred for 24 hours. The reaction mixture was neutralized to pH = 7 using concentrated HCl, and evaporated to dryness under reduced pressure. The resulting residues and salts were dissolved in $H_2O$ and dialyzed in a 3.5 KDa MWCO dialysis cassette against $H_2O$ for 3 days, with $H_2O$ changes every 8 hours for the first 24 hours, followed

by every 12 hours subsequently. The contents of the cassette were removed and filtered through a 0.2 μM filter. The resulting solution was lyophilized to yield a white solid.

**Synthesis of Poly(GalNAc-co-Ala) and poly(Mannose-co-Ala):** As previously described. (*20*, *35*).

**Glycopolypeptide Molecular Weight Analysis with Aqueous GPC:** Gel permeation chromatography (GPC) was carried out in aqueous 0.1M $NaNO_3$ + 0.01M $NaN_3$ or PBS using an OHpak SB-803 HQ Shodex column with the dimensions 8.0 x 300 mm a particle size of 6 μm connected in series with a DAWN multiangle laser light scattering (MALLS) detector and an Optilab T-rEX differential refractometer (both from Wyatt Technology), dn/dc values were obtained for each injection by assuming 100% mass elution from the columns.

**Glycopolypeptide GPC Molecular Weights, Dispersities, and $^1$H NMR Glycosylated Serine:Alanine Ratios:**

poly(Mannose-co-Ala): $M_n$=18.9 KDa, Đ = 1.51, 2.4:1
poly(GalNAc-co-Ala): $M_n$=27.1 KDa, Đ = 1.24, 1.2:1
poly(M6Pn-co-Ala)$_{short}$: $M_n$=9.75 KDa, Đ = 1.32, 1:1.6
poly(M6Pn-co-Ala)$_{long}$: $M_n$=37.1 KDa, Đ = 1.42, 1:0.9
poly(M6P-co-Ala)$_{short}$: $M_n$=8.20 KDa, Đ = 1.58, 1:1.2
poly(M6P-co-Ala)$_{long}$: $M_n$=24.7 KDa, Đ = 1.75, 1:1.2

**Representative Procedure for Polymer N-terminal Biotinylation:** To 1.0 mg of poly(M6Pn)$_{short}$ ($M_n$ = 9.7 KDa, 103 nmoles) was added PBS (0.5 mL), and 40 equiv. Biotin-Sulfo-NHS (1.8 mg). The reaction was allowed to incubate for 12 hours at room temperature, then purified with a NAP-25 column, eluting with water. The eluent was then dialyzed against $H_2O$ for 48 hours, with 6 water changes. Yield: 896 μg. The resulting material was dissolved in 231 μL PBS to make a 400 μM stock solution.

**Representative Procedure for Polymer N-terminal Azide-Functionalization:** To 1.0 mg of poly(M6Pn)$_{short}$ ($M_n$ = 9.7 KDa, 103 nmoles) was added PBS (0.5 mL), and 50 equiv. NHS-$PEG_4$-$N_3$ (100 μL of a 20 mg/mL stock) was added. The reaction was allowed to incubate for 12 hours at room temperature, then purified with a NAP-25 column, eluting with water. The eluent was then dialyzed against water for 48 hours, with 6 water changes.

**Representative Procedure for Polymer N-terminal BCN-Functionalization:** To 500 μg of poly(M6Pn)$_{short}$ ($M_n$ = 9.7 KDa, 51.5 nmoles) was added PBS (1.0 mL) and 25 equiv. BCN-NHS (360 μL of a 1 mg/mL stock in DMSO). The reaction was allowed to incubate for 12 hours at room temperature, then purified with a NAP-25 column, eluting with water. The eluent was then dialyzed against $H_2O$ for 48 hours, with 6 water changes. Yield: 424 μg.

**Representative Procedure for Antibody Labeling with BCN-NHS (Cetuximab):** 1 mL of a 2 mg/mL solution of cetuximab was concentrated with a 30K spin filter and subsequently diluted to 1000 μL with PBS. 100 μg (25 equiv.) of NHS-BCN in DMSO (1 mg/mL solution, 100 uL) was

added, and the reaction was allowed to incubate at rt overnight. After incubation, the reaction mixture was filtered and diluted eight times using a 500 µL, 30 KDa Amicon Centrifugal Filter.

**Representative Procedure for Antibody Labeling with NHS-PEG$_4$-N$_3$ (Cetuximab):** 1 mL of a 2 mg/mL solution of cetuximab was concentrated with a 30K spin filter and subsequently diluted with 1000 µL PBS. 137 µg (25 equiv., 14 µL) of NHS-PEG4-N3 in DMSO (10 mg/mL, 137 uL) was added, and the reaction was allowed to incubate at rt overnight. After incubation, the reaction mixture was filtered and diluted eight times using a 500 µL, 30 KDa Amicon Centrifugal Filter.

**Representative Procedure for Antibody-Glycopolypeptide Conjugation:** To poly(M6Pn)$_{short}$-N$_3$ (136 µg, 20 equiv.) was added ctx-BCN (100 µg, 50 µL in PBS) and the reaction was allowed to incubate for 3 days at room temperature. The reaction mixture was filtered 9X with a 50 KDa Amicon Centrifugal Filter, then resuspended in 100 µL 1X PBS to give a 5.94 µM solution in PBS (89% recovery). Protein concentration was determined by $A_{280}$ absorbance.

**Cell Lines:** Cells were grown in T75 flasks (Thermo Fisher) and maintained at 37 °C and 5% $CO_2$. K562 and Jurkat cells were grown in RPMI supplemented with 10% fetal bovine serum (FBS) and 1% penicillin/streptomycin. THP-1 were grown in RPMI supplemented with 10% FBS, 1% penicillin/streptomycin, and 0.05 mM 2-mercaptoethanol. HeLa, MDA-MB-361, HEK293, A549, BT474, and MDA-MB-231 were grown in DMEM supplemented with 10% fetal bovine serum (FBS) and 1% penicillin/streptomycin. HDLM-2 were grown in RPMI supplemented with 20% heat-inactivated FBS and 1% penicillin/streptomycin. HeLa and K562 cells stably expressing dCas9-KRAB were a generous gift from Michael Bassik, Stanford University.

**General Procedure for NeutrAvidin-647 Uptake Experiments:** Cells (70% confluent in 24-well plate for adherent cells, $1\times10^6$ cells/mL for suspension cells) were incubated in complete growth medium supplemented with 500 nM NA-647, or NA-647 and 2 µM glycopolypeptide. Addition was performed sequentially, with NA-647 added first followed by glycopolypeptide and immediate transfer to 37 °C.

**General Procedure for Protein Uptake and Degradation Experiments:** Cells (70% confluent in 24-well plate for adherent cells, $2\times10^6$ cells/mL for suspension cells) were incubated in complete growth medium supplemented with 50 nM target protein, or 50 nM target protein and 25 nM of each antibody. Addition was performed sequentially, with target protein added first followed by secondary antibodies, followed by primary antibodies, and subsequent immediate transfer to 37 °C.

**CRISPRi Screen Procedure:** The hCRISPRi-v2 library was a generous gift from Jonathan Weissman (Addgene ID #83969). K562 cells stably expressing dCas9-KRAB were infected with the 104,535 sgRNA library described in Horlbeck *et al*. (*25*), targeting the transcriptional start sites of 18,905 annotated genes at a redundancy of 5 sgRNA/start site. Infectivity was titrated such as to transduce the library at an MOI of 0.3-0.4. Cells were selected with puromycin for 96 h and then allowed to expand in puromycin-free media for 48 h. Staining and FACS was performed within seven days of completion of puromycin selection. On the day of sorting, two replicates of $50x10^6$ library-infected cells ($4\times10^6$ cells/mL) were incubated with NA-647 (500 nM)

and poly(M6Pn)$_{long}$ (2 μM) for 1 hour at 37 °C. Cells were washed three times with PBS at 4 °C. Cells were then resuspended in PBS with Sytox Green (according to manufacturer's specifications) and FACS sorted using a BD Aria II. Intact, viable cells were selected by gating on FSC/SSC and Sytox Green channels. A population of cells representing the bottom 15% of the fluorescence distribution in the NA-647 channel was then selected for and sorted. Sorting was conducted until 25x10$^6$ events had been processed, corresponding to a ~250-fold library coverage. Sorted cells were then pelleted and frozen for subsequent downstream processing. Aliquots of 50x10$^6$ unsorted cells from each replicate were also pelleted and frozen down in parallel for normalization.

**CRISPRi Screen DNA Extraction and Data Analysis:** Frozen cell pellets were thawed and genomic DNA extraction was performed using either the QIAamp DNA Blood Maxi Kit (for unsorted samples) or the Sigma GeneElute Mammalian Genomic DNA Miniprep kit (for sorted samples) according to manufacturer's specifications. The sgRNA-encoding regions were amplified via nested PCR and sequenced on an Illumina NextSeq500. Alignment of sequencing reads to sgRNA library and statistical comparison of positively selected genes in sorted vs. unsorted samples was performed using MaGeCK (*36*). MaGeCK returned a statistical score for gene enrichment in the sorted population and genes were ranked by a positive selection score corresponding to the -log(PosScore). GO enrichment analysis was performed using GOrilla (*37*).

**Generation of CRISPRi Knockdown Cell Lines:** K562 or HeLa cell stably expressing dCas9-KRAB were infected with lentivirus encoding guide sgRNAs obtained from the CRISPRi screen. Lentivirus was produced by co-transfection of HEK-293T cells with a lentiviral transfer vector and packaging plasmids (pGag/pol, pREV, pTAT, pVSVG). Transfection was performed using Lipofectamine 2000 reagent as recommended by the manufacturer. Viral supernatants were collected 48 h following transfection, filtered through a 0.45 μm filter, and added to target cells (400 μL viral supernatant/well in a 6-well plate) along with polybrene (8 μg/mL). 48-hours post infection, cell media was replaced and cells were placed under puromycin selection (2 μg/mL).

sgRNA guides:
*CI-M6PR* 5'-GAGGTGAGCGCGGCTCGACT-3'
*EXOC1 5'*-GGGCGGACAGACGAGCTGAC-3'
*EXOC2 5'*-GGGCGGAAGTGAGGTGCCGG-3'

**Flow Cytometry for Surface Staining and Uptake Measurements:** For protein uptake experiments in suspension cell lines, cells were incubated for the indicated time with proteins and conjugates, then washed three times with PBS at 4 °C. Cells were then incubated with either Sytox Green or Sytox Red according to the manufacturer's specifications for 15 minutes on ice. For protein uptake experiments in adherent cell lines, cells were incubated for the indicated time with proteins and conjugates, then washed two times quickly with PBS and lifted with trypsin. Cells were transferred to a 96-well V-bottom plate and washed three times with PBS, then incubated with either Sytox Green or Sytox Red according to the manufacturer's specifications for 15 minutes on ice.

For surface staining experiments, adherent cells were lifted with non-enzymatic cell dissociation buffer (Gibco) and transferred to a 96-well V-bottom plate, and suspension cells were transferred to a 96-well V-bottom plate. After washing three times with 0.5% BSA in PBS, cells were incubated with primary antibody for 30 minutes on ice. Cells were subsequently washed three times with 0.5% BSA in PBS, then incubated with secondary antibodies for 30 minutes on ice. After incubation, cells were washed three times with 0.5% BSA in PBS and incubated with

either Sytox Green or Sytox Red according to the manufacturer's specifications for 15 minutes on ice. Flow cytometry was performed on either a BD-Accuri C6 Plus or DxP FACScan flow cytometer, and analysis was performed using the FlowJo software package. Gating was performed on single cells and live cells.

**Cell Surface Degradation Experiment:** Adherent cells (70% confluency for 24-hour experiments, 50% confluency for 48-hour experiments) were treated with antibodies or conjugates in complete growth media. At the indicated time, cells were washed three times with DPBS, then lysed as detailed below. Suspension cells were suspended in complete growth media in a flat bottom plate, and at the indicated time transferred to a 96-well V-bottom plate and washed three times with PBS, then lysed as detailed below.

**Western Blotting:** Cell culture experiments with adherent cells conducted in 24-well plates were washed three times with DPBS, then lysed with RIPA buffer supplemented with protease inhibitor cocktail (Roche), phosphatase inhibitor cocktail (Cell Signaling Technologies) and 0.1% benzonase (Millipore-Sigma) on ice for 30 minutes. The lysates were spun at 21,000*g* for 15 minutes at 4 °C and protein concentration was determined using BCA assay (Pierce). Suspension cell lines were transferred to a 96-well V-bottom plate, washed three times with PBS, then lysed with RIPA buffer supplemented as above. Adherent cells in 6-well plates were washed three times with DPBS then lysed with 1X Laemmli buffer containing protease inhibitor cocktail (Roche) and phosphatase inhibitor cocktail (Cell Signaling Technologies). Lysates were then sonicated on ice using a microtip sonicator for 30 seconds, with 10 second sonication intervals and rest intervals, and protein concentration was determined using BCA assay (Pierce). Equal amounts of lysates were separated by sodium dodecyl sulfate-polyacrylamide gel electrophoresis (4-12% Bis-Tris gel), then transferred to a nitrocellulose membrane. After transfer, the membrane was stained for total protein using REVERT Total Protein Stain (LI-COR), then blocked in TBS-T with 5% non-fat dried milk or Odyssey Blocking Buffer (TBS) (LI-COR) for 1 hour at room temperature with gentle shaking. Membranes were incubated overnight with primary antibody at 4 °C with gentle shaking, then washed three times with TBS-T for five minutes each. The membrane was then incubated with 800CW goat anti-mouse IgG, 800CW goat anti-rabbit IgG, 800CW donkey anti-goat IgG, or 680LT goat anti-rabbit IgG secondary antibodies (1:10,000) in Odyssey Blocking Buffer (TBS) for one hour at room temperature with gentle shaking. Membranes were washed three times with TBS-T, then imaged using an OdysseyCLxImager (LI-COR). Quantification of band intensities was performed using Image Studio Software (LI-COR).

**Confocal microscopy:** A Nikon A1R confocal microscope equipped with a Plan Fluor 60x oil immersion 1.30–numerical aperture objective was used. This instrument is equipped with a 405-nm violet laser, 488-nm blue laser, 561-nm green, and a 639-nm red laser.

**Antibodies and Usage:**

| Antibody | Source (#) | Usage and dilution |
|---|---|---|
| Rabbit anti-EGFR | CST (D38B1) | WB, 1:1000 |
| Goat anti-EGFR | R&D Systems (AF231) | WB, 1:1000 |
| Mouse anti-CD71 | Bio-Rad (VMA00037) | WB, 1:1000 |
| Rabbit anti-PD-L1 | CST (E1L3N) | WB, 1:500 |
| Mouse anti-Vinculin | Bio-Rad (V284) | WB, 1:1000 |

| | | |
|---|---|---|
| Mouse anti-α-Tubulin | Millipore Sigma (T5168) | WB, 1:5000 |
| Rabbit anti-EXOC1 | Abcam (ab118798) | WB, 1:2500 |
| Rabbit anti-CIM6PR | CST (D3V8C) | WB, 1:1000 |
| Mouse anti-CD71 | BioXCell (BE0023) | Functional |
| Mouse anti-PD-L1 | BioXCell (BE0285) | Functional |
| Mouse anti-mCherry | Biorbyt (orb66657) | Functional |
| Mouse anti-ApoE4 | Novus Biologicals (4E4) | Functional |
| Goat anti-Mouse IgG | Jackson ImmunoResearch (115-005-062) | Functional |
| Mouse anti-biotin-Alexa Fluor 488 | Jackson ImmunoResearch (200-542-211) | Functional |
| Cetuximab | Eli Lilly | Flow cytometry, Functional |
| Mouse anti-CIM6PR | Abcam (2G11) | Flow cytometry, 1:500 |
| Goat anti-mouse IgG-Alexa Fluor 488 | Jackson ImmunoResearch (115-545-008) | Flow cytometry, 1:375 |
| Goat anti-mouse IgG-Alexa Fluor 647 | Jackson ImmunoResearch (115-605-071) | Flow cytometry, 1:375 |
| Goat anti-human IgG-Alexa Fluor 647 | Jackson ImmunoResearch (109-605-003) | Flow cytometry, 1:375 |

**Mass Spectrometry:**

**Sample Preparation:** Samples were prepared for proteomic analysis using a previously described method with methanol precipitation to extract proteins, followed by tryptic digestion (*38*). Briefly, HeLa cells from each treatment condition were lysed by suspension in 6 M guanidine, total protein concentration was measured using BCA (Thermo Fisher Scientific), and 100 µg of protein was extracted via precipitation in 90% methanol for each sample. Supernatants were decanted and protein pellets were suspended in a buffer comprising 8 M urea, 100 mM tris pH 8, 10 mM tris(2-carboxyethyl)phosphine, and 40 mM chloroacetamide. Following incubation at room temperature for 30 minutes, samples were diluted to 1.5 M urea with 100 mM tris pH 8 and digested with trypsin (50:1 protein to enzyme, Promega, Madison, WI) overnight. Sample cleanup was performed by first quenching with formic acid to a final pH of ~2, followed by desalting over a polystyrene-divinylbenzene solid phase extraction (PS-DVB SPE) cartridge (Phenomenex). Samples were dried with vacuum centrifugation following desalting, and peptide mass was assayed using peptide colorimetric assay (Fisher).

**LC-MS/MS:** All samples were resuspended in 0.2% formic acid in water at ~ 500 ng/µL, and 500 ng of total peptide mass was injected on column for each sample. Peptides were separated over a 25 cm EasySpray reversed phase LC column (75 µm inner diameter packed with 2 µm, 100 Å, PepMap C18 particles, Thermo Fisher Scientific). The mobile phases (A: water with 0.2% formic acid and B: acetonitrile with 0.2% formic acid) were driven and controlled by a Dionex Ultimate 3000 RPLC nano system (Thermo Fisher Scientific). Gradient elution was performed at 300 nL/min. Mobile phase B was increased to 5% over 6 min, followed by an increase to 40% at 76 min, a ramp to 90% B at 77 min, and a wash at 90% B for 10 min. Flow was then ramped back to 0% B over the course of 1 min, and the column was re-equilibrated at 0% B for 12 min, for a total analysis of 100 minutes. Eluted peptides were analyzed on an Orbitrap Fusion Tribrid MS system (Thermo Fisher Scientific). Precursors were ionized using an EASY-Spray ionization source (Thermo Fisher Scientific) source held at +2.2 kV compared to ground, and the column was held at 40 °C. The inlet capillary temperature was held at 275 °C. Survey scans of peptide precursors were collected in the Orbitrap from 350-1500 Th with an AGC target of 1,000,000, a maximum

injection time of 50 ms, and a resolution of 120,000 at 200 m/z. Monoisotopic precursor selection was enabled for peptide isotopic distributions, precursors of z = 2-5 were selected for data-dependent MS/MS scans for 2 seconds of cycle time, and dynamic exclusion was set to 45 seconds with a ±10 ppm window set around the precursor monoisotope. An isolation window of 0.7 Th was used to select precursor ions with the quadrupole. MS/MS scans were collected using HCD at 30 normalized collision energy (nce) with an AGC target of 30,000 and a maximum injection time of 25 ms. Mass analysis was performed in the linear ion trap using the “Rapid” scan speed while scanning from 200-1500 Th.

**Data Analysis:** Raw data were processed using MaxQuant version 1.6.3.4 (*39*), and tandem mass spectra were searched with the Andromeda search algorithm (*40*). Oxidation of methionine and protein N-terminal acetylation were specified as variable modifications, while carbamidomethylation of cysteine was set as a fixed modification. A precursor ion search tolerance of 20 ppm and a product ion mass tolerance of 0.3 Da were used for searches, and two missed cleavages were allowed for full trypsin specificity. Peptide spectral matches (PSMs) were made against a target-decoy human reference proteome database downloaded from Uniprot. Peptides were filtered to a 1% false discovery rate (FDR) and a 1% protein FDR was applied according to the target-decoy method (*41*). Proteins were identified and quantified using at least one peptide (razor + unique), where razor peptide is defined as a non-unique peptide assigned to the protein group with the most other peptides (Occam's razor principle). Proteins were quantified and normalized using MaxLFQ (*42*) with a label-free quantification (LFQ) minimum ratio count of 1. LFQ intensities were calculated using the match between runs feature, and MS/MS spectra were required for LFQ comparisons. For quantitative comparisons, protein intensity values were log2 transformed prior to further analysis, and missing values were imputed from a normal distribution with width 0.3 and downshift value of 1.8 (i.e., default values) using the Perseus software suite (*43*). Significance calculations were performed using a two-tailed t-test with heteroscedastic variance (performed in Microsoft Excel).

## Supplemental Figures

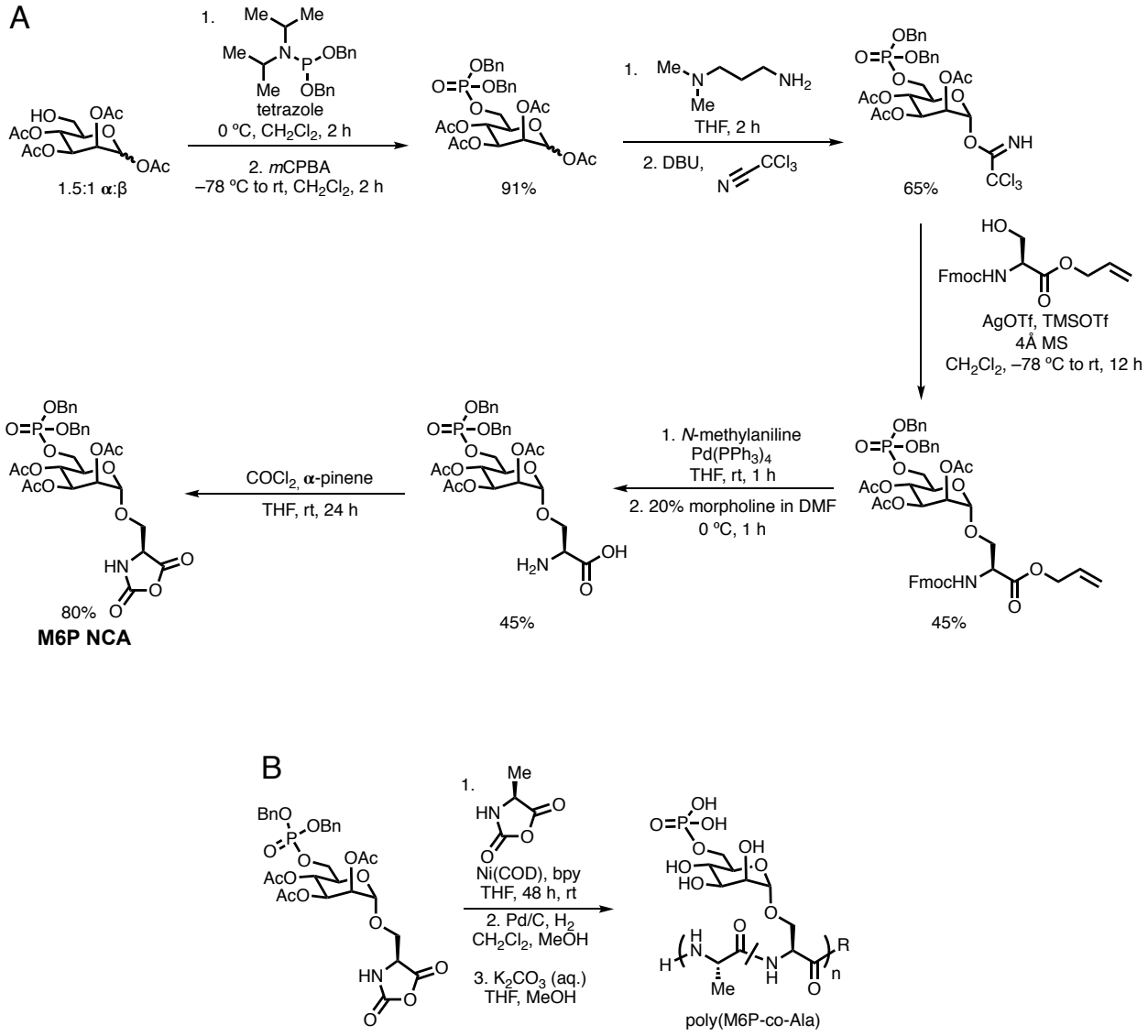


**Fig. S1. Synthesis of mannose-6-phosphate (M6P) glycopolypeptides.** (A) Synthetic route to mannose-6-phosphate-serine *N*-carboxyanhydride (NCA). (B) General synthetic scheme for poly(M6P) glycopolypeptides. Polymerization reactions were carried out in a $N_2$ glovebox for 48 hours in THF.

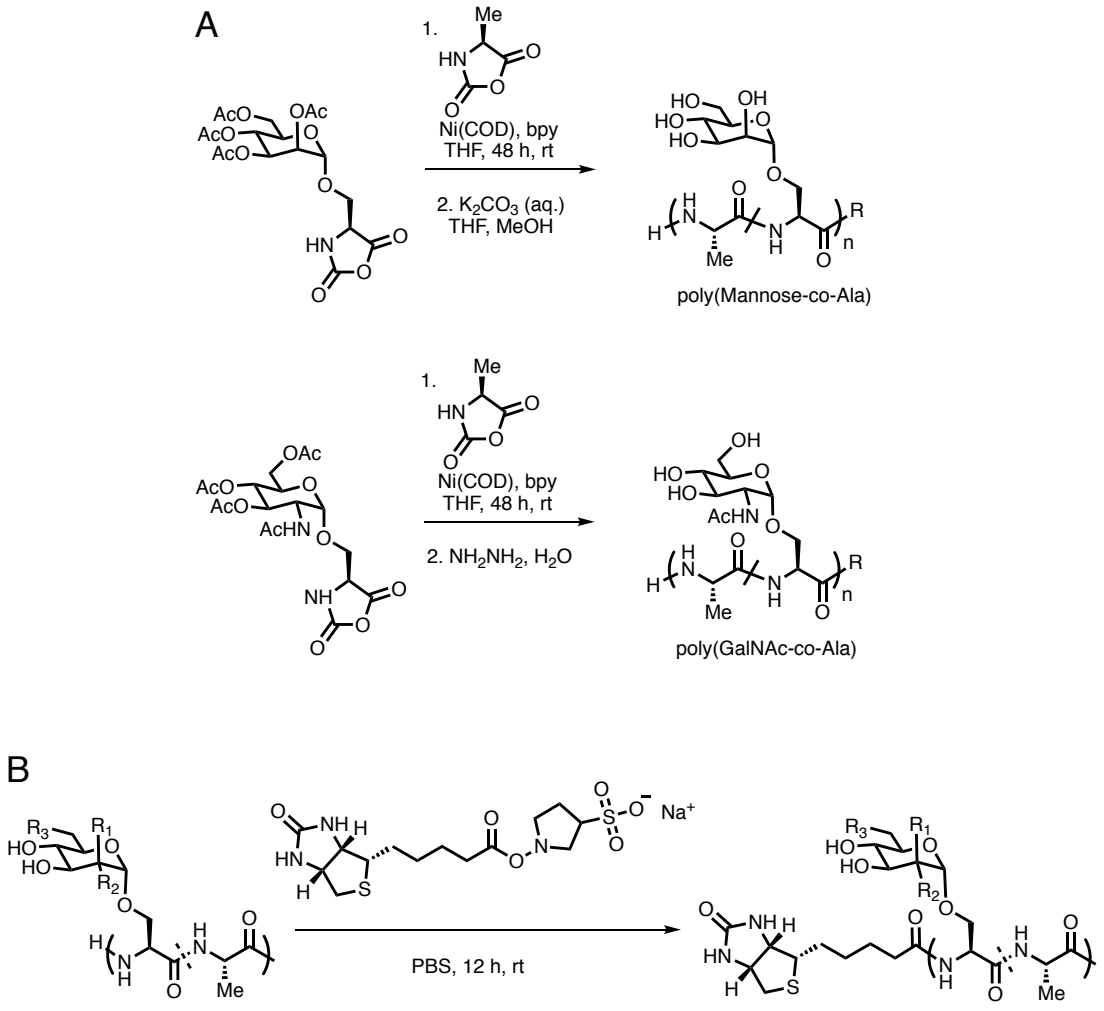


**Fig. S2. Synthesis of poly(Mannose-co-Ala), poly(GalNAc-co-Ala) and N-terminal biotinylation of glycopolypeptides.** (A) General synthetic schemes for polymerization of Mannose-NCA and GalNAc-NCA. (B) General scheme for biotinylation of glycopolypeptides with sulfo-NHS biotin. Biotinylation reactions were performed in 1X PBS at room temperature overnight.

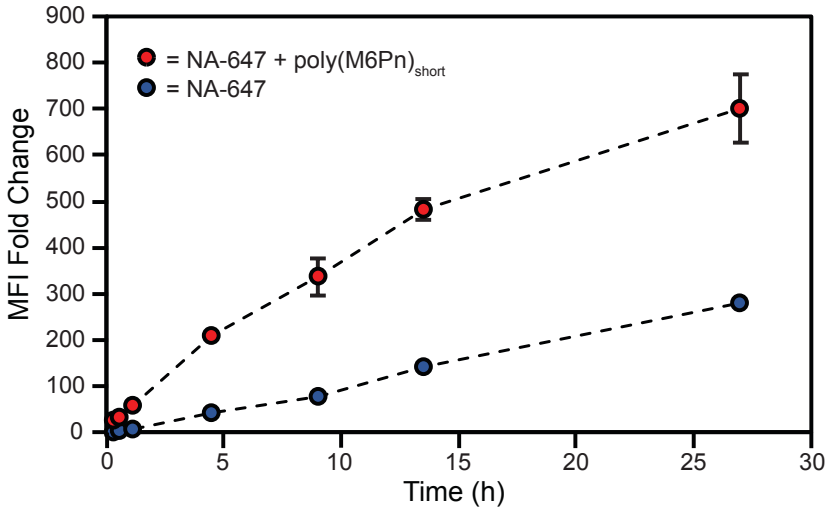


**Fig. S3. CIM6PR-mediated NeutrAvidin (NA-647) uptake is continuous over time in K562 cells.** K562 cells were incubated at 37 °C in full-serum media with 500 nM NA-647 or 500 nM NA-647 and 2 μM poly(M6Pn)$_{short}$ for the indicated time, then washed and analyzed by live cell flow cytometry. The mean fluorescence intensity (MFI) was measured relative to background fluorescence from untreated K562 cells. Error bars represent standard deviation of three independent experiments.

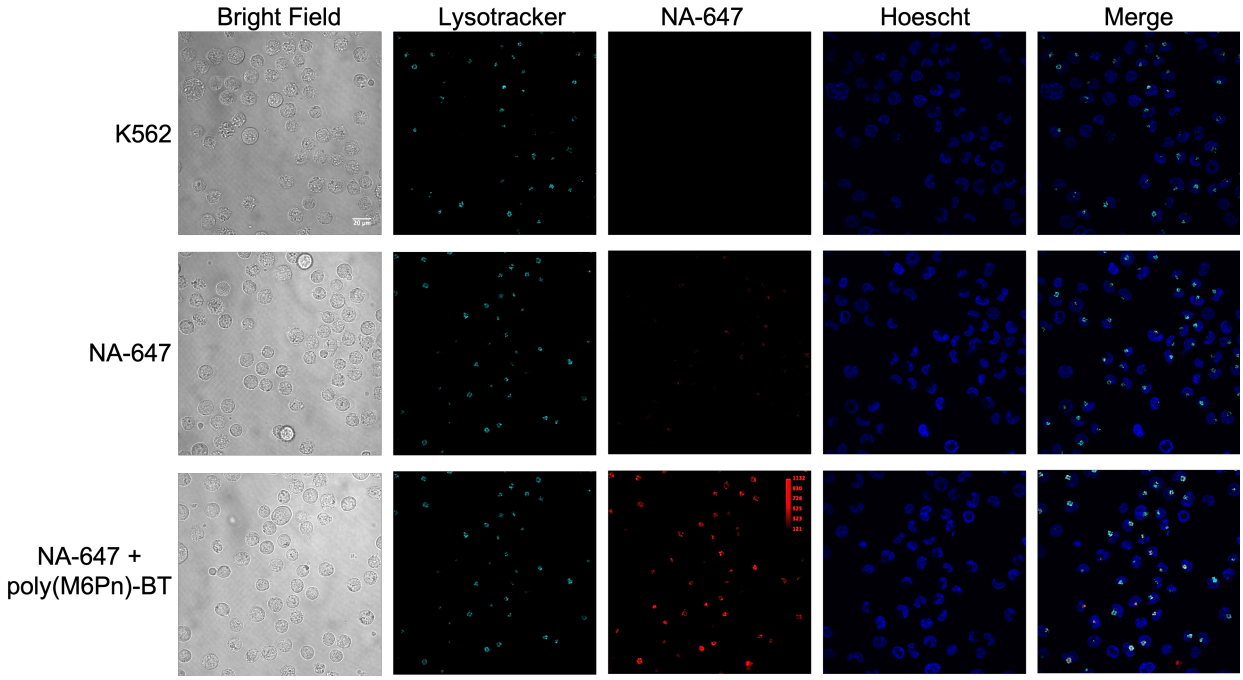


**Fig. S4. Biotiylated poly(M6Pn) LYTACs direct NeutrAvidin-647 (NA-647) to lysosomes in K562 cells.** K562 cells were incubated with PBS, 500 nM NA-647, or 500 nM NA-647 and 2 μM biotinylated poly(M6Pn)$_{short}$ for 1 h in full-serum media. NA-647 (red) colocalized with acidic endosomes and lysosomes as labeled with Lysotracker Green (turquoise). Scale bar is 20 μM. Fluorescence intensity is normalized in the NA-647 channel for all images.

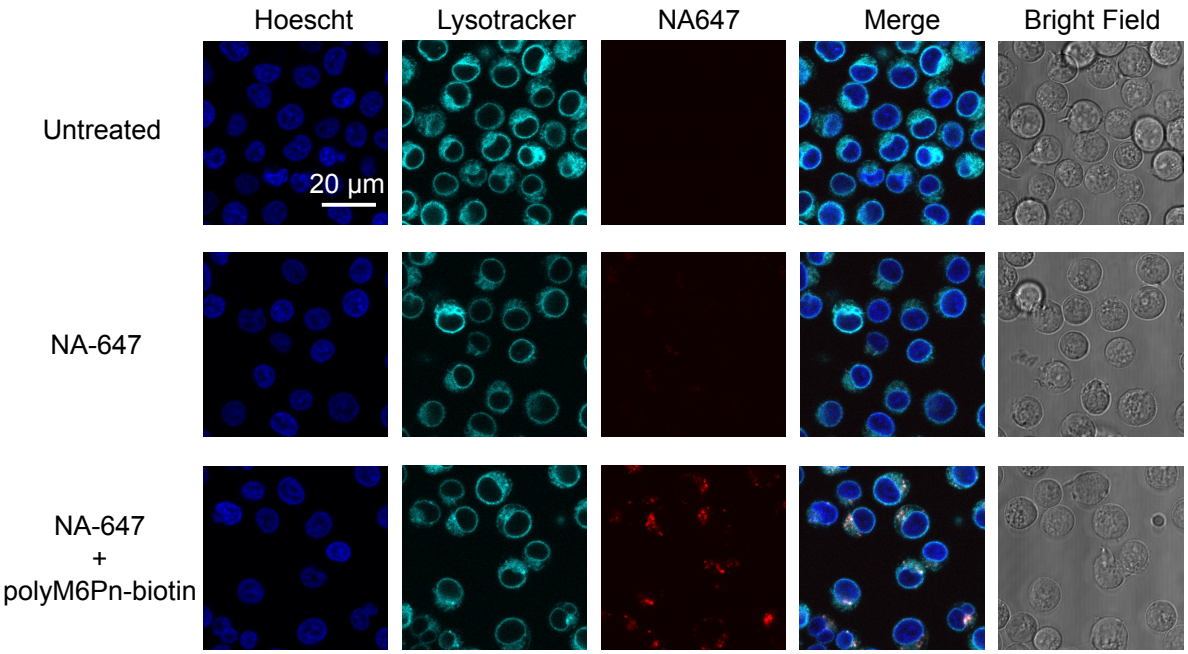


**Fig. S5. Biotiylated poly(M6Pn) LYTACs direct NeutrAvidin-647 (NA-647) to lysosomes in Jurkat cells.** Jurkat cells were incubated with PBS, 500 nM NA-647, or 500 nM NA-647 and 2 μM biotinylated poly(M6Pn)$_{short}$ for 0.5 h in full-serum media. NA-647 (red) colocalized with acidic endosomes and lysosomes as labeled with Lysotracker Green (turquoise). Scale bar is 20 μM. Fluorescence intensities are normalized for all images.

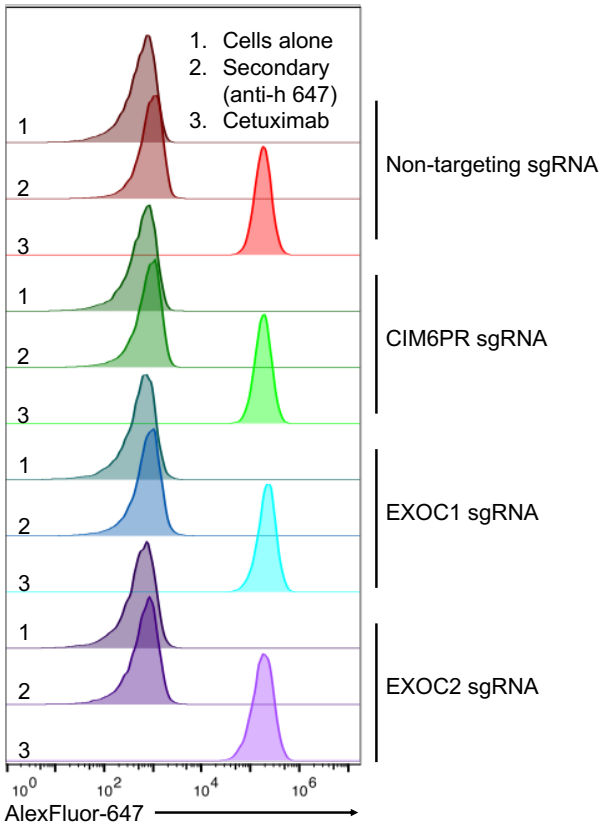


**Fig. S6. EGFR surface localization is unchanged in EXOC1 and EXOC2 knockdown HeLa cells.** Cetuximab binds equally to dCas9-KRAB HeLa cells transfected with non-targeting sgRNA and cells transfected with sgRNA against CI-M6PR, EXOC1, or EXOC2, indicating no change in EGFR surface transport. Cells were subjected to live cell flow cytometry using cetuximab followed by an anti-human AlexaFluor-647 conjugated anti-human (anti-h 647) secondary antibody.

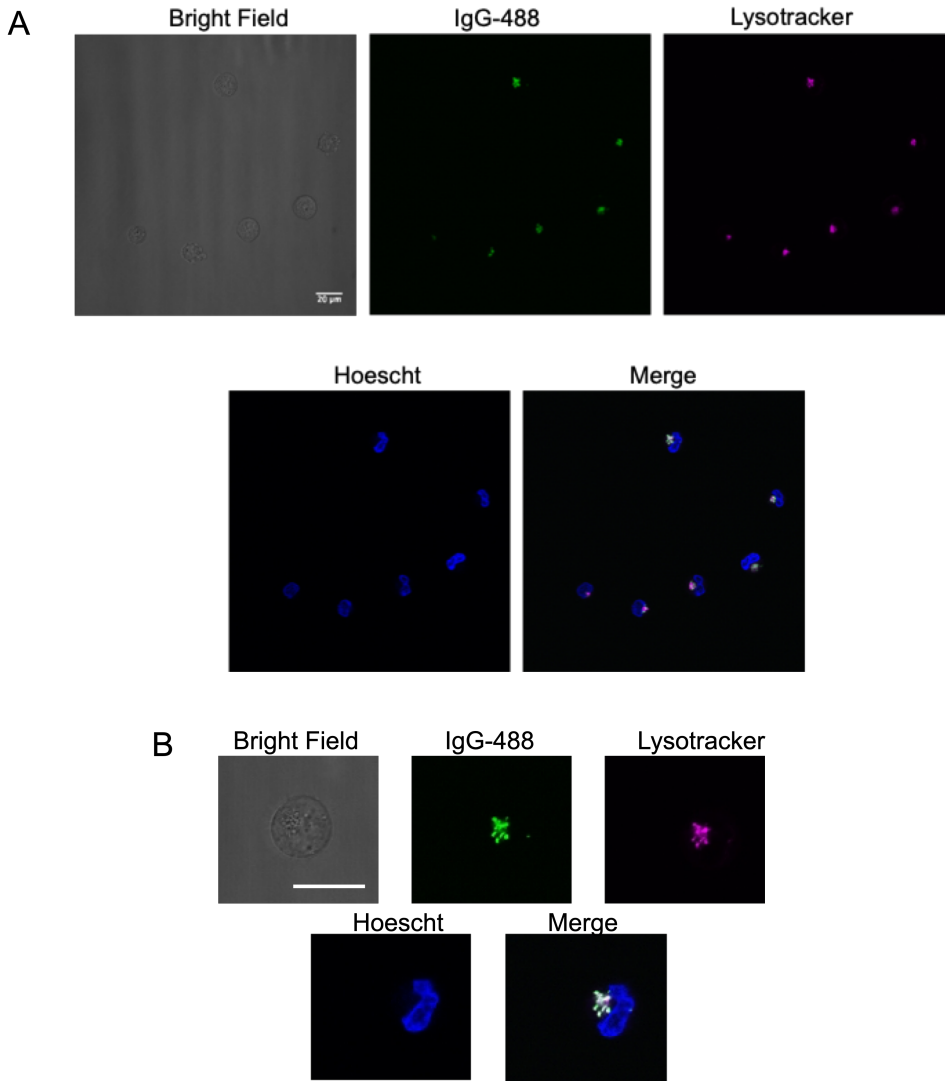


**Fig. S7. Ab-1 mediates uptake of soluble proteins to lysosomes.** (A) K562 cells were incubated with PBS, 50 nM *m*-IgG-488, or 50 nM *m*-IgG-488 and 25 nM Ab-1 for 1 h in full-serum media at 37 °C. IgG-488 (green) colocalized with acidic endosomes and lysosomes as labeled with Lysotracker Red (magenta). (B) Expanded view of K562 cells containing IgG-488 and Lysotracker Red. Scale bars are 20 μm.

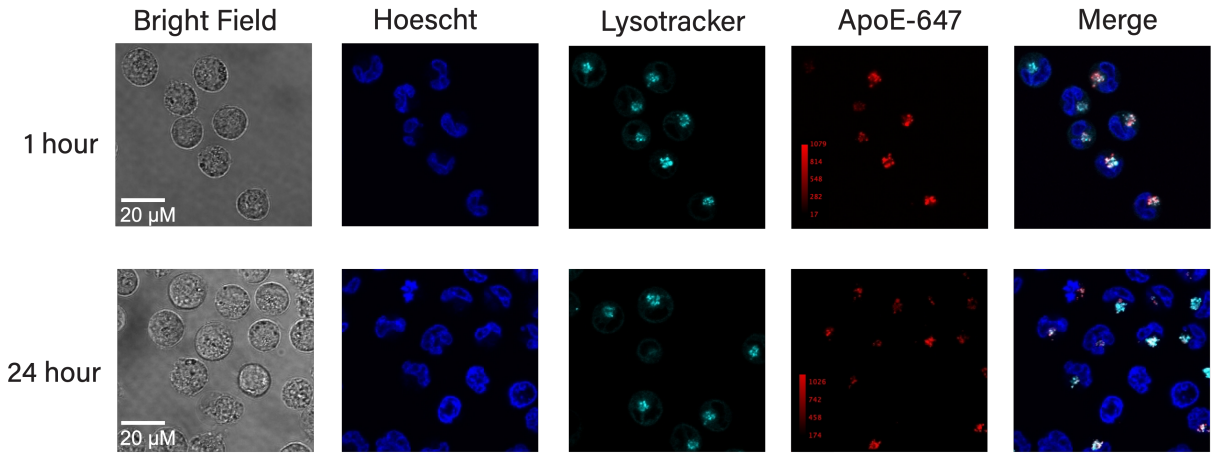


**Fig. S8. Ab-1 mediates uptake of ApoE4-647 to lysosomes at both 1 and 24 hours.** (A) K562 cells were incubated with PBS, 50 nM ApoE4-647, 25 nM anti-ApoE4, and 25 nM Ab-1 for 1 h or 24 h in full-serum media at 37 °C. AlexaFluor-647 signal (red) colocalizes with acidic endosomes and lysosomes as labeled with Lysotracker Green (turquoise).

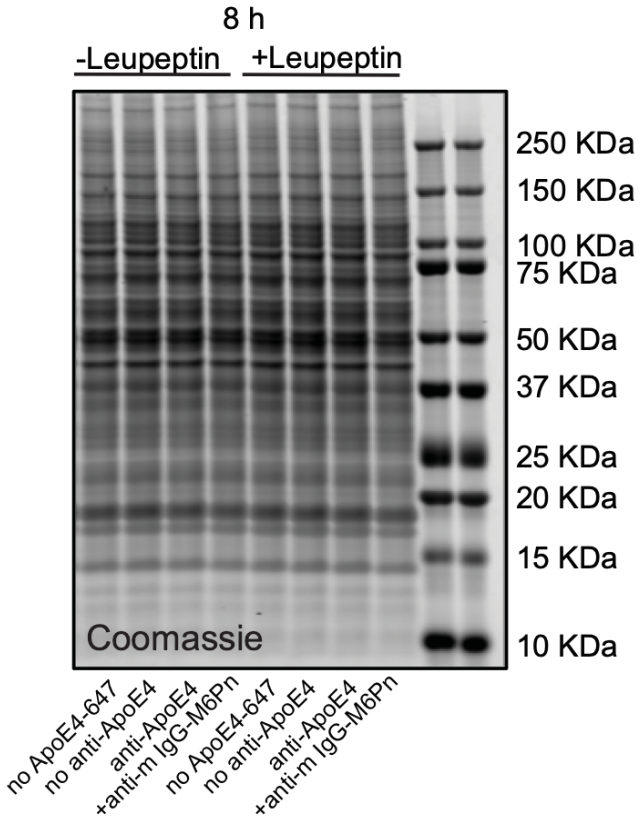


**Fig. S9. Total protein levels for leupeptin inhibition of apoE4 degradation in K562 cells, corresponding to lanes shown in Figure 3K.** Total protein was visualized by Coomassie stain.

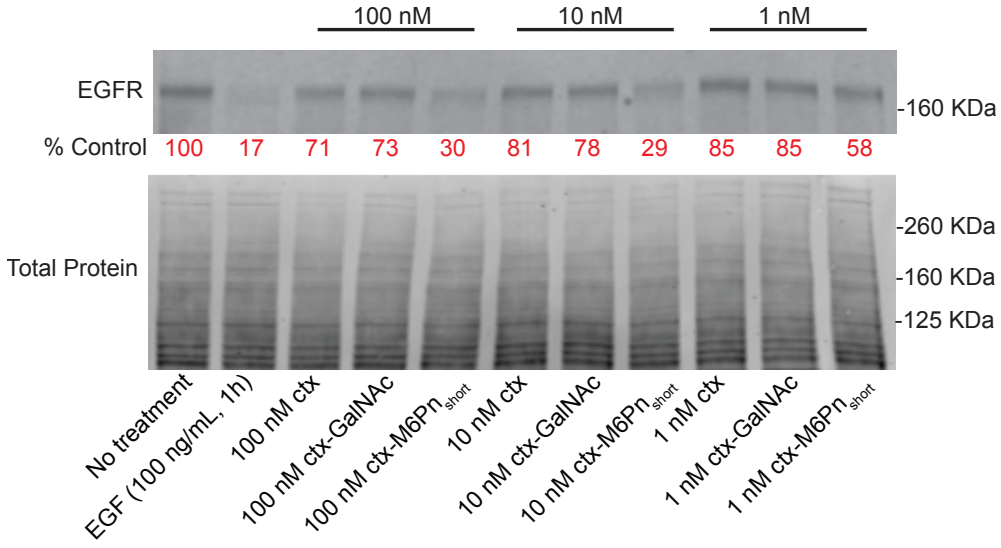


**Fig. S10. LYTAC-mediated EGFR degradation occurs in a concentration dependent manner.** HeLa cells were incubated with 100 nM, 10 nM, or 1 nM conjugates for 24 hours in full serum media. After 24 hours, cells were lysed, and total EGFR levels were measured by Western blot. Percent control was calculated by densitometry and normalized to total protein.

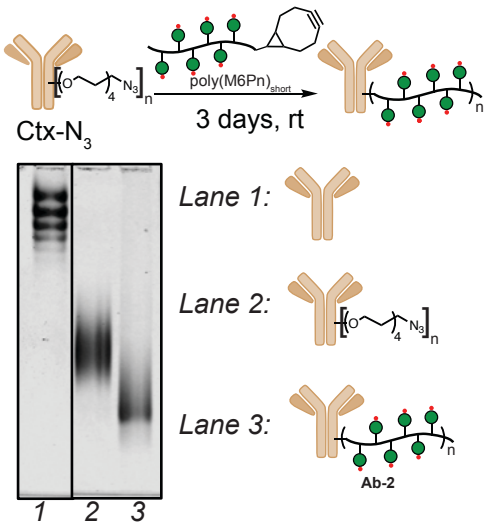


**Fig. S11. Synthesis of Ab-2.** Cetuximab was labeled with NHS-PEG$_4$-N$_3$, then incubated with BCN-functionalized poly(M6Pn)$_{short}$ for 3 days at room temperature. Reaction progress was monitored by native gel electrophoresis and visualized with Coomassie stain.

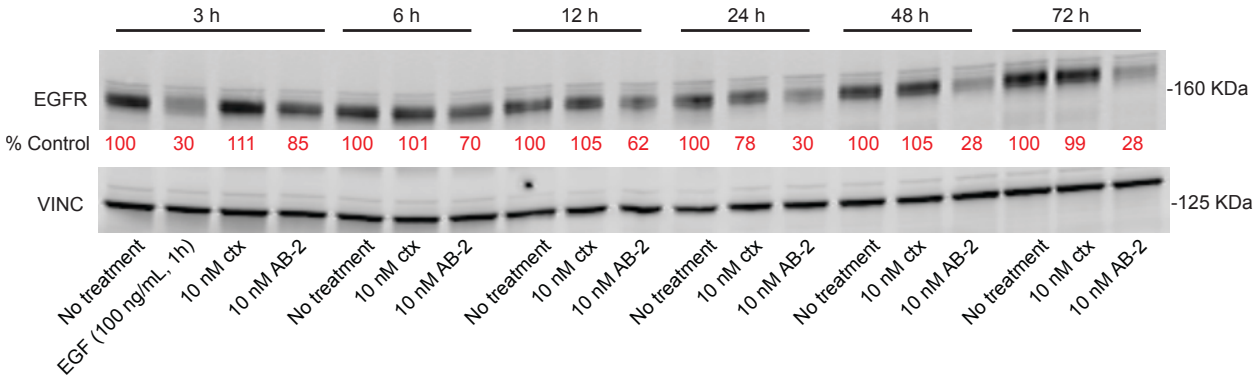


**Fig. S12. LYTAC-mediated EGFR degradation increases over time.** HeLa cells were incubated with conjugates for the indicated time, then washed and lysed. Total EGFR levels were assayed by Western blot and degradation was calculated by densitometry normalized to vinculin loading control.

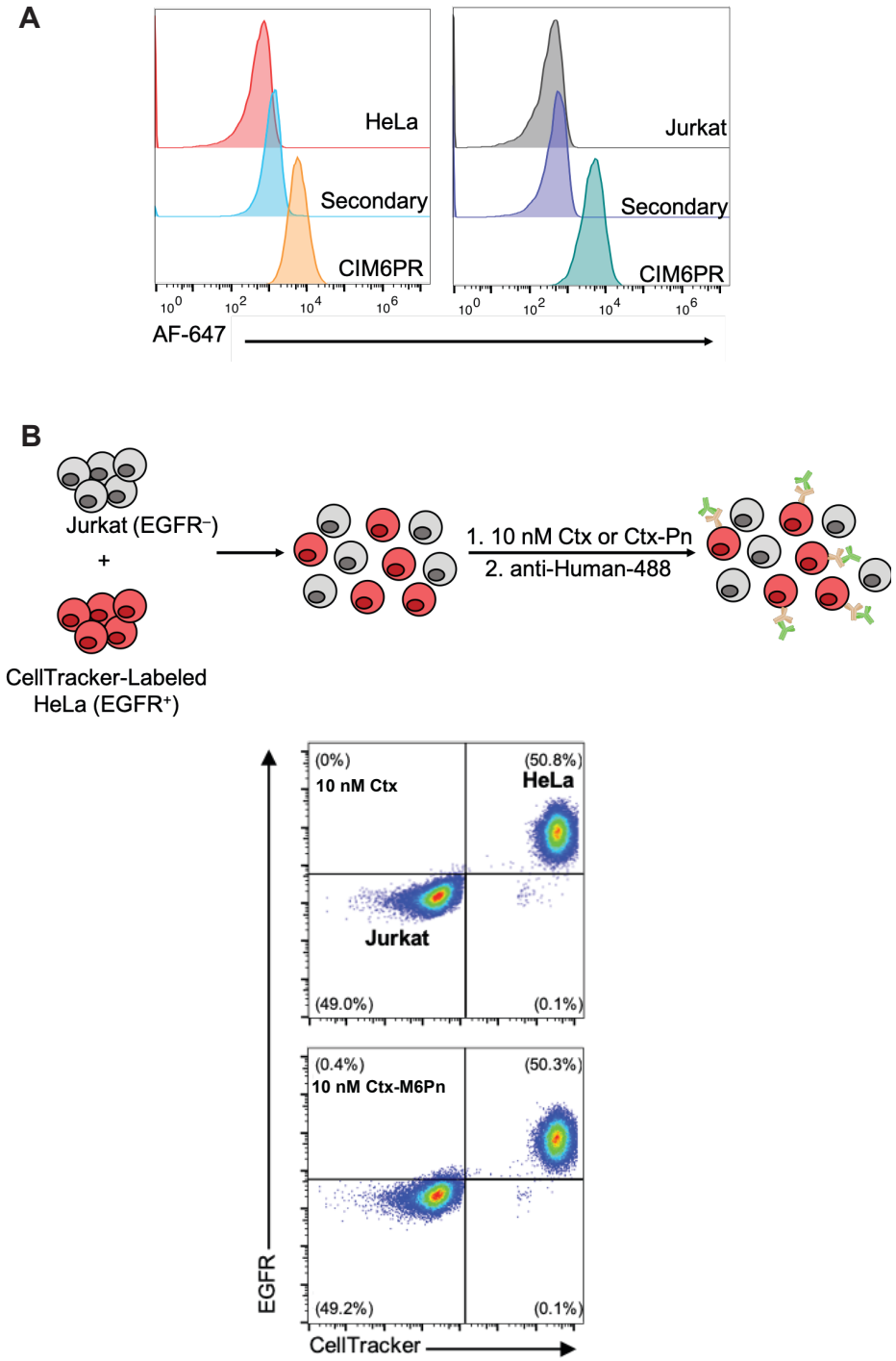


**Fig. S13. Mixed-cell assay demonstrates that ctx-M6Pn binding specificity is comparable to ctx.** (A) Cell surface CIM6PR levels on HeLa cells ($CIM6PR^+EGFR^+$) and Jurkat cells ($CIM6PR^+EGFR^-$) was measured by live cell flow cytometry. HeLa and Jurkat exhibited similar levels of cell surface CIM6PR. (B) HeLa cells were lifted and labeled with CellTracker Deep Red, then mixed in a 1:1 ratio with Jurkat cells. The mixed cell sample was stained with 10 nM cetuximab or ctx-M6Pn conjugate and anti-human 488, then subjected to live cell flow cytometry. Ctx and ctx-M6Pn exhibit equivalent binding to HeLa cells, and ctx-M6Pn exhibits < 1% increased binding to Jurkat cells relative to ctx.

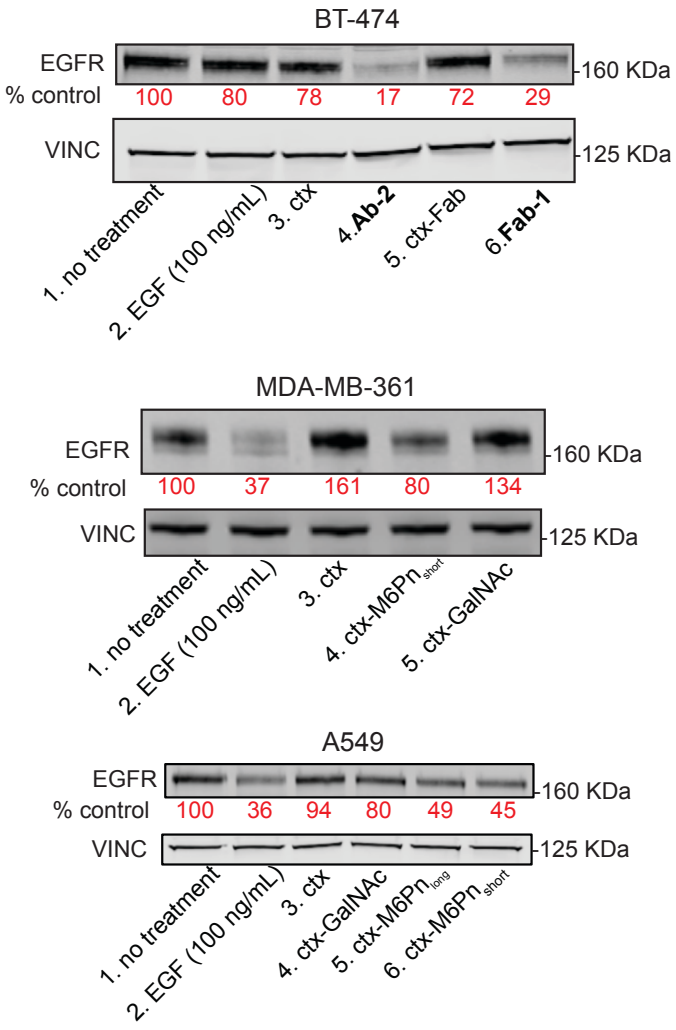


**Fig. S14. EGFR is degraded in multiple cell lines.** BT-474, MDA-MB-361, or A549 cells were incubated with 20 nM conjugates, then washed and lysed. Total EGFR amounts were assayed by Western blot, and degradation was measured by densitometry normalized to vinculin loading control.

| | Ab-2 (ctx-M6Pn) | |
|---|---|---|
| | ***Downregulated*** | |
| | Fold Change | p value |
| DHPR | -3.08 | 0.023 |
| TFDP1 | -2.98 | 0.039 |
| 8ODP | -1.82 | 0.019 |
| CD99 | -1.8 | 0.051 |
| UBXN6 | -1.55 | 0.043 |
| WDR11 | -1.38 | 0.049 |
| BAG5 | -1.35 | 0.015 |
| AGAP3 | -1.31 | 0.036 |
| SCO2 | -1.21 | 0.017 |
| ORC2 | -1.08 | 0.015 |
| | ***Upregulated*** | |
| | Fold Change | p value |
| CCD57 | 3.82 | 0.046 |
| PGM2L | 2.72 | 0.012 |
| NFIB | 2.48 | 0.003 |
| ALKB5 | 2.21 | 0.029 |
| COPRS | 2.13 | 5.4E-05 |
| IGKC | 1.99 | 0.009 |
| FRYL | 1.99 | 0.024 |
| DESP | 1.12 | 0.0006 |

| | Cetuximab | |
|---|---|---|
| | ***Downregulated*** | |
| | Fold Change | p value |
| TF2B | -2.37 | 0.008 |
| HIF1N | -1.54 | 0.042 |
| | ***Upregulated*** | |
| | Fold Change | p value |
| CCD57 | 3.82 | 0.036 |
| IGKC | 3.15 | 0.032 |
| NFIB | 2.43 | 0.006 |
| PO2F1 | 2.06 | 0.03 |
| NRBP | 2.01 | 0.011 |

**Fig. S15. Examples of proteins with differential abundance following treatment of HeLa cells with ctx. or ctx.-M6Pn.** Untreated, ctx-treated, or Ab-2-treated HeLa cells were lysed, digested, and analyzed by quantitative proteomics. Depicted are exemplary hits with fold change values reported relative to untreated samples. Proteins highlighted in gray were found in both ctx and Ab-2 treated cells. For a full list, see Supplementary Data 2.

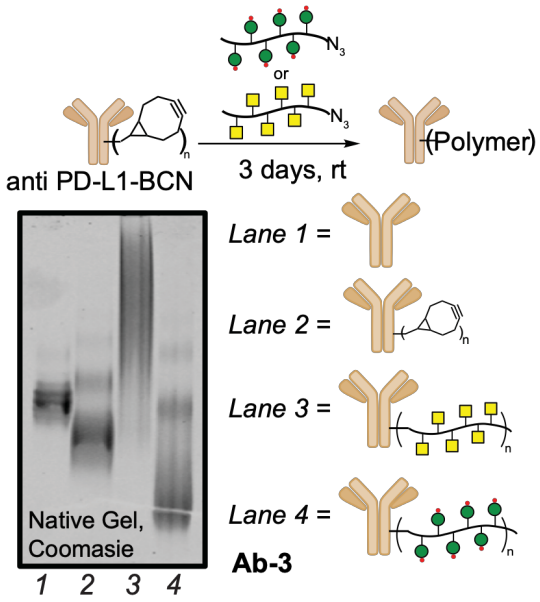


**Fig. S16. Synthesis of anti PD-L1 glycopolypeptide conjugates.** Anti-PD-L1 was non-specifically labeled with BCN, then incubated with poly(M6Pn)$_{short}$ for 3 days at room temperature. Reaction progress was monitored by native gel electrophoresis and visualized by Coomassie stain.

## NMR and FTIR Spectra

$^{1}$H NMR
400 MHz
$CDCl_3$

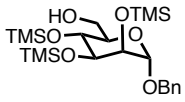


**M6Pn-I2**




$^{13}$C NMR
101 MHz
$CDCl_3$

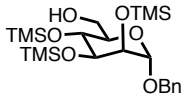

$^{1}$H NMR
400 MHz
$CDCl_3$

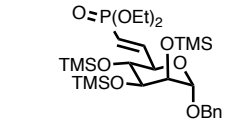


**M6Pn-I3**




$^{13}$C NMR
101 MHz
$CDCl_3$

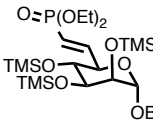

$^{31}P$ NMR
162 MHz
$CDCl_3$

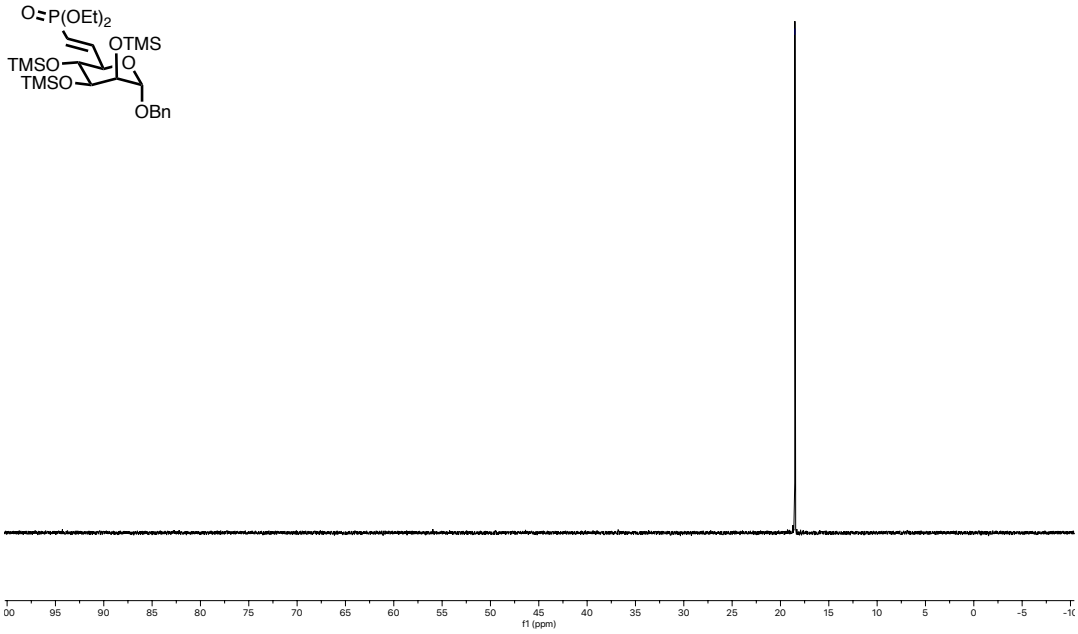

$^{1}$H NMR
400 MHz
$CDCl_3$

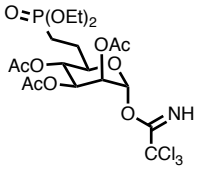


**M6Pn-I4**




$^{13}$C NMR
101 MHz
$CDCl_3$

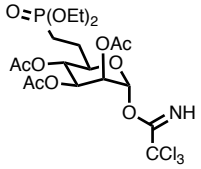

$^{31}P$ NMR
162 MHz
$CDCl_3$

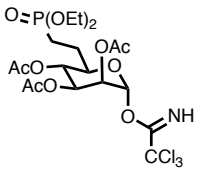

$^{1}$H NMR
400 MHz
$CDCl_3$

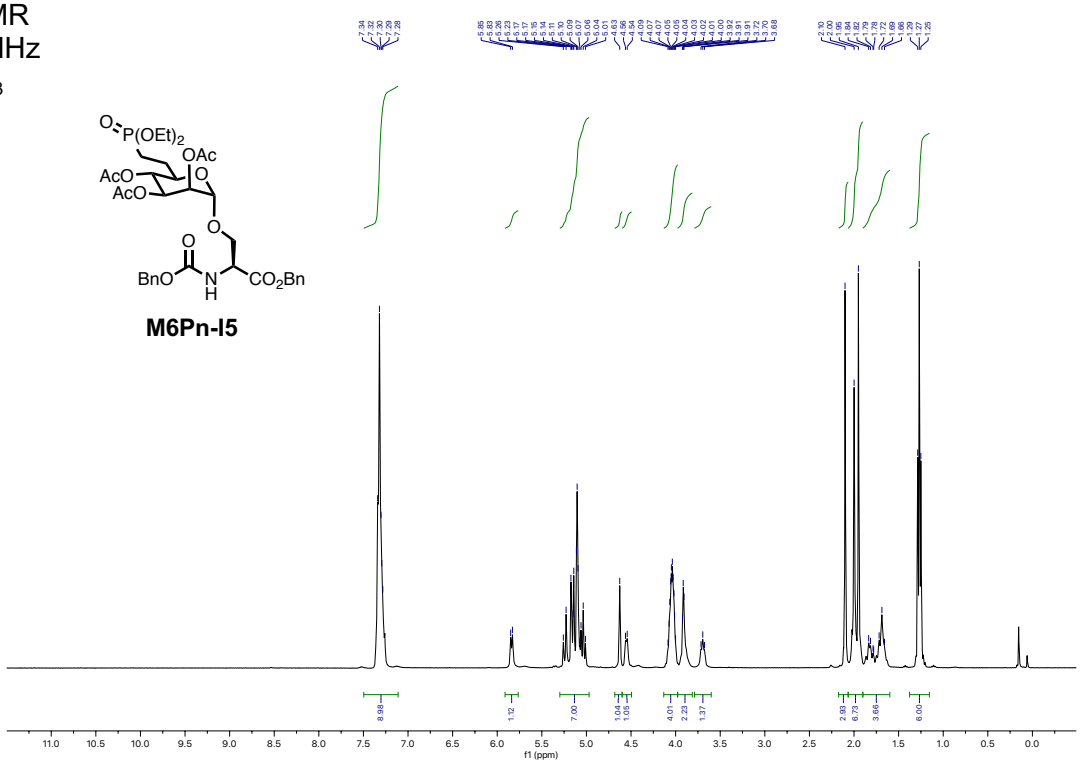


**M6Pn-I5**

$^{13}$C NMR
101 MHz
$CDCl_3$

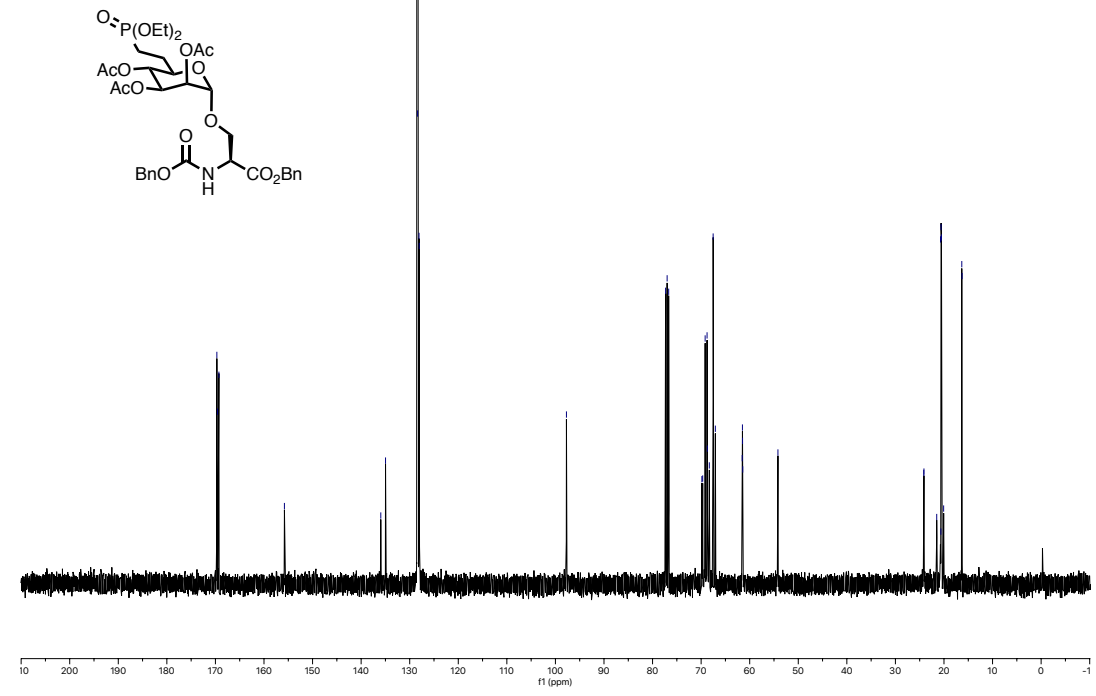

$^{31}P$ NMR
162 MHz
$CDCl_3$

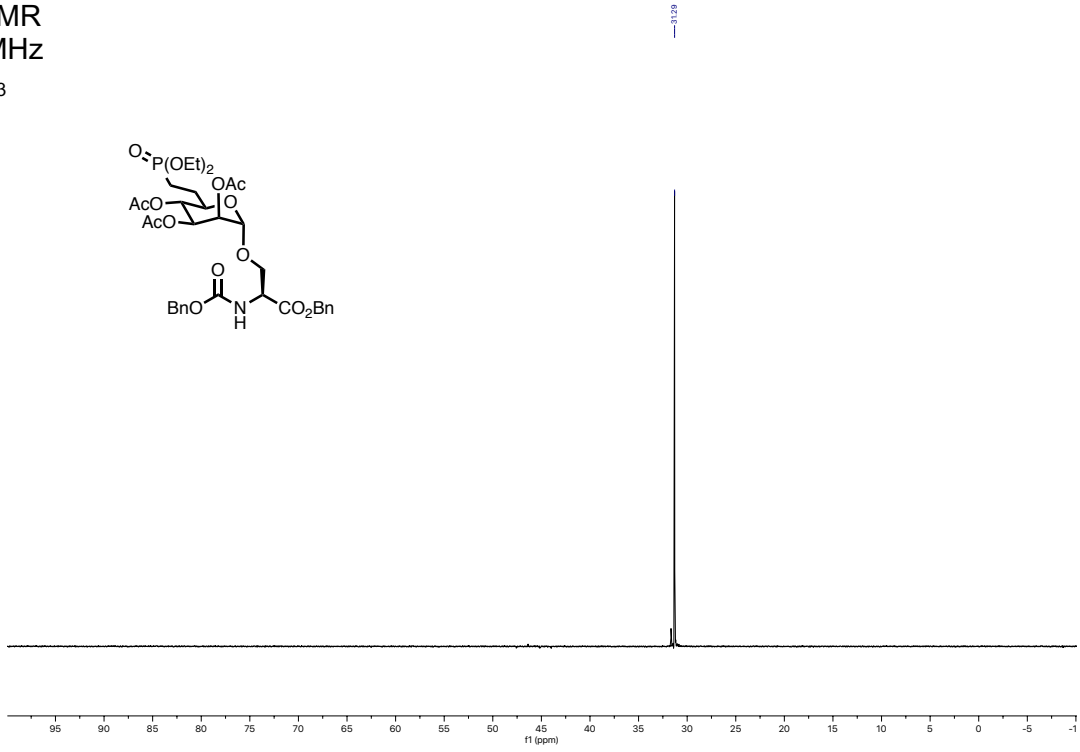

$^{1}$H NMR
400 MHz
$CDCl_3$

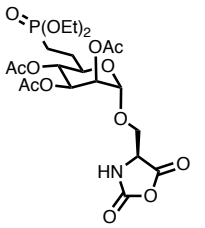


**M6Pn-NCA**




$^{13}$C NMR
101 MHz
$CDCl_3$

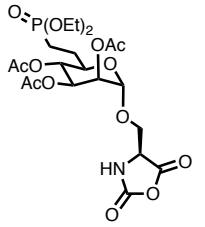

$^{31}P$ NMR
162 MHz
$CDCl_3$

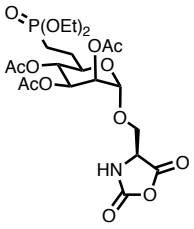

$^{1}$H NMR
400 MHz
$CDCl_3$

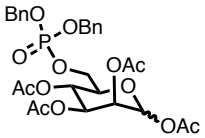


**M6P-I2**




$^{13}$C NMR
101 MHz
$CDCl_3$

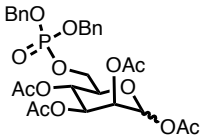

$^{31}P$ NMR
162 MHz
$CDCl_3$

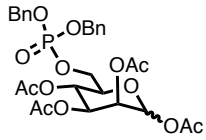

$^{1}$H NMR
400 MHz
$CDCl_3$

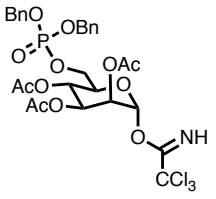


**M6P-I3**




$^{13}$C NMR
101 MHz
$CDCl_3$

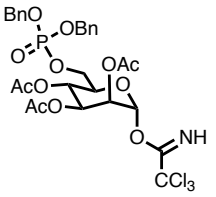

$^{31}P$ NMR
162 MHz
$CDCl_3$

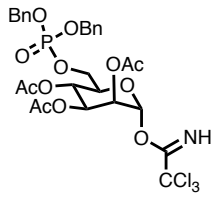

$^{1}$H NMR
400 MHz
$CDCl_3$

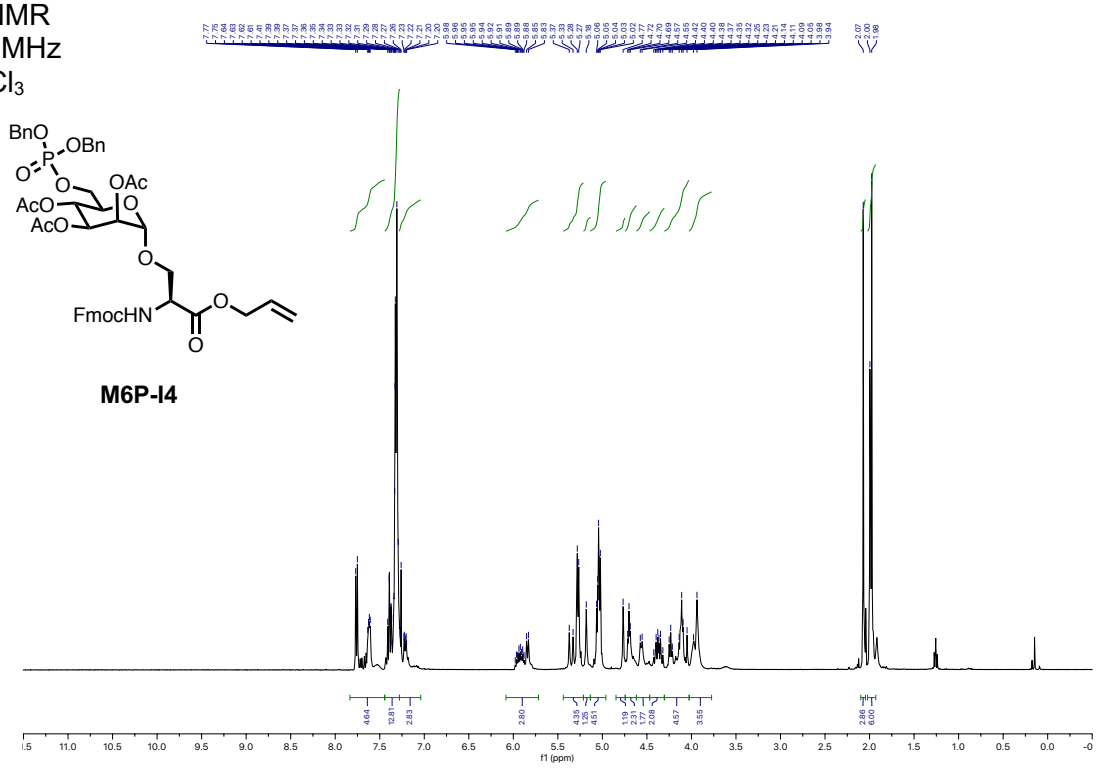


**M6P-I4**

$^{13}$C NMR
101 MHz
$CDCl_3$

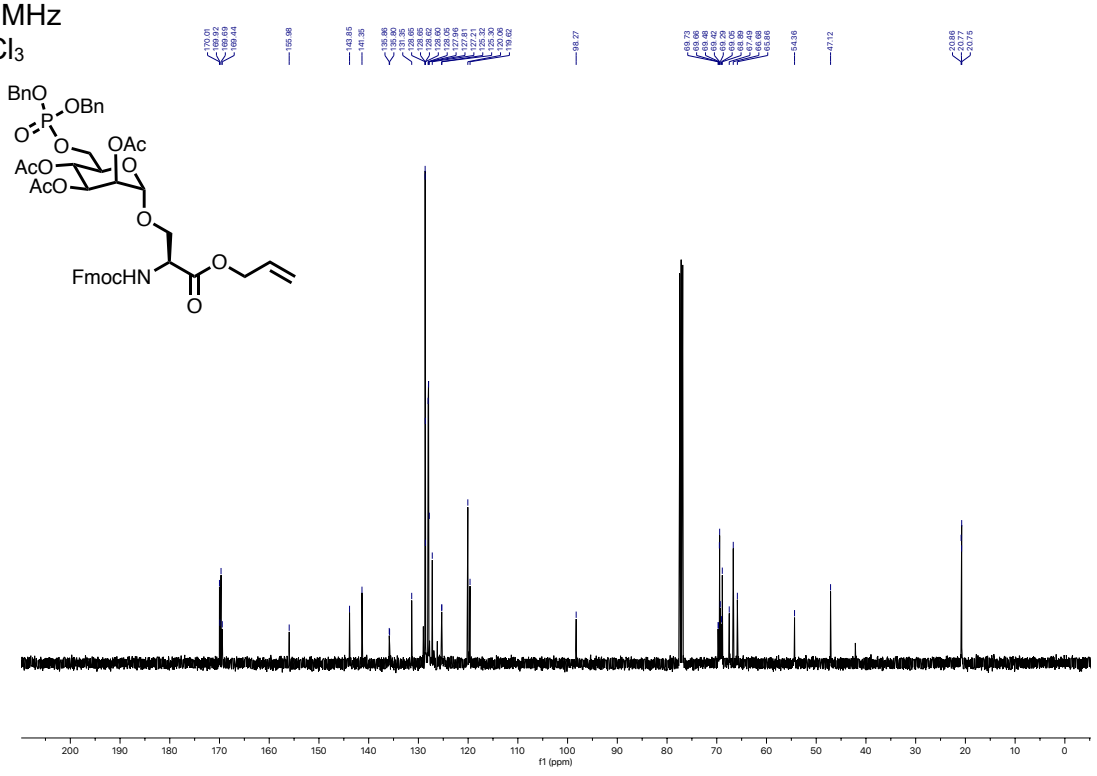

$^{31}P$ NMR
162 MHz
$CDCl_3$

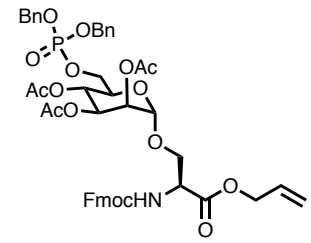

$^{1}$H NMR
400 MHz
$CD_3OD$

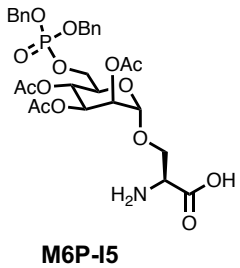


**M6P-I5**




$^{13}$C NMR
101 MHz
$CD_3OD$

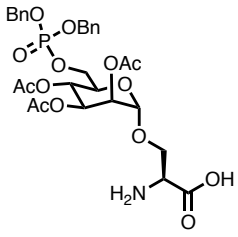

$^{31}P$ NMR
162 MHz
$CD_3OD$

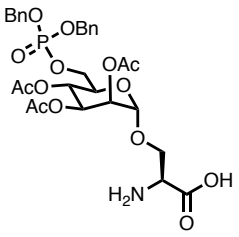

$^{1}$H NMR
400 MHz
$CDCl_3$

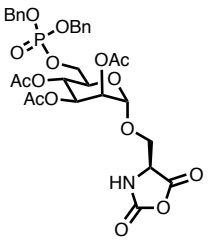


**M6P-NCA**




$^{13}$C NMR
101 MHz
$CDCl_3$

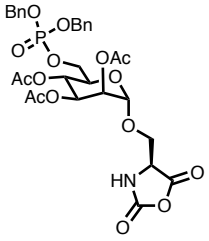

$^{31}P$ NMR
162 MHz
$CDCl_3$

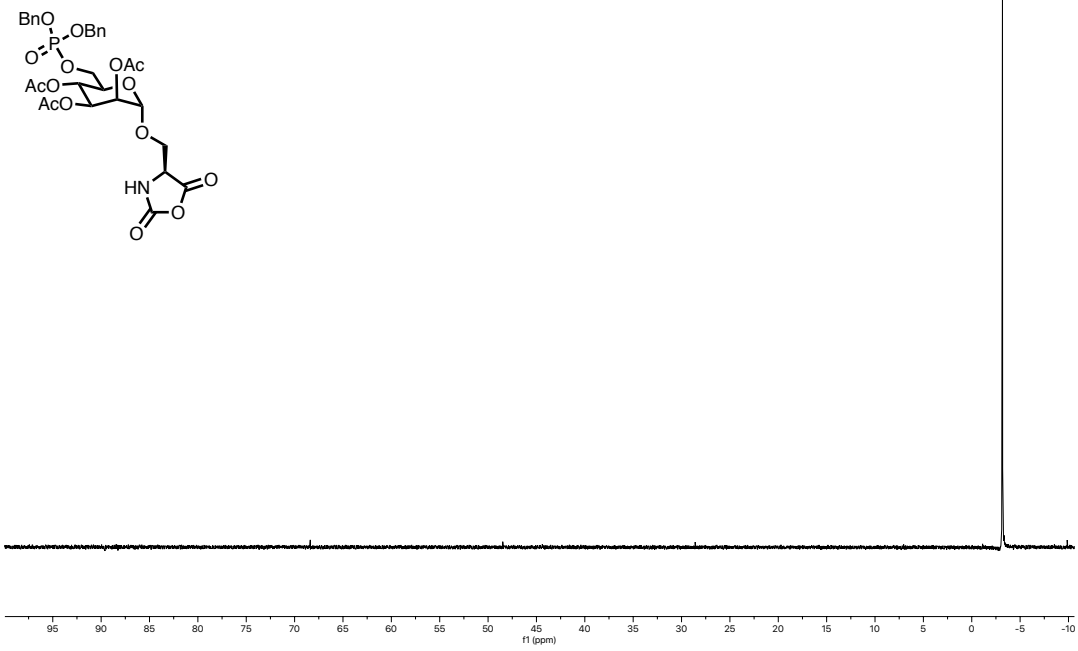

$^{1}$H NMR
600 MHz
$D_2O$

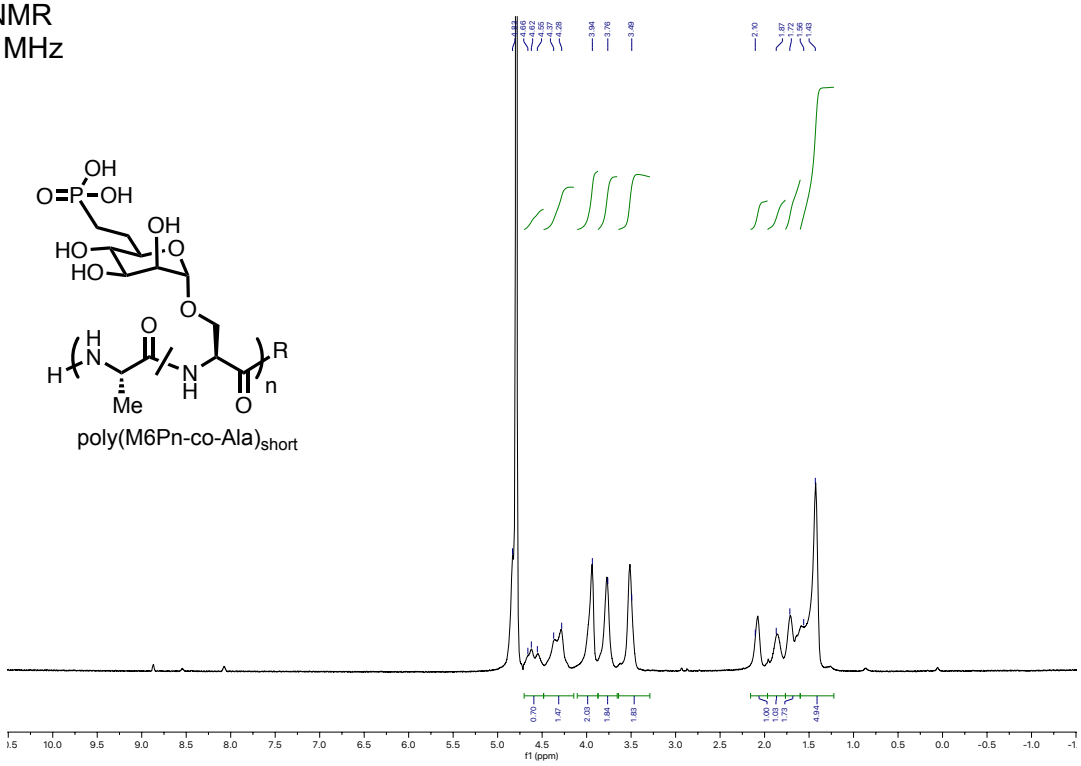


$^{31}$P NMR
162 MHz
$D_2O$

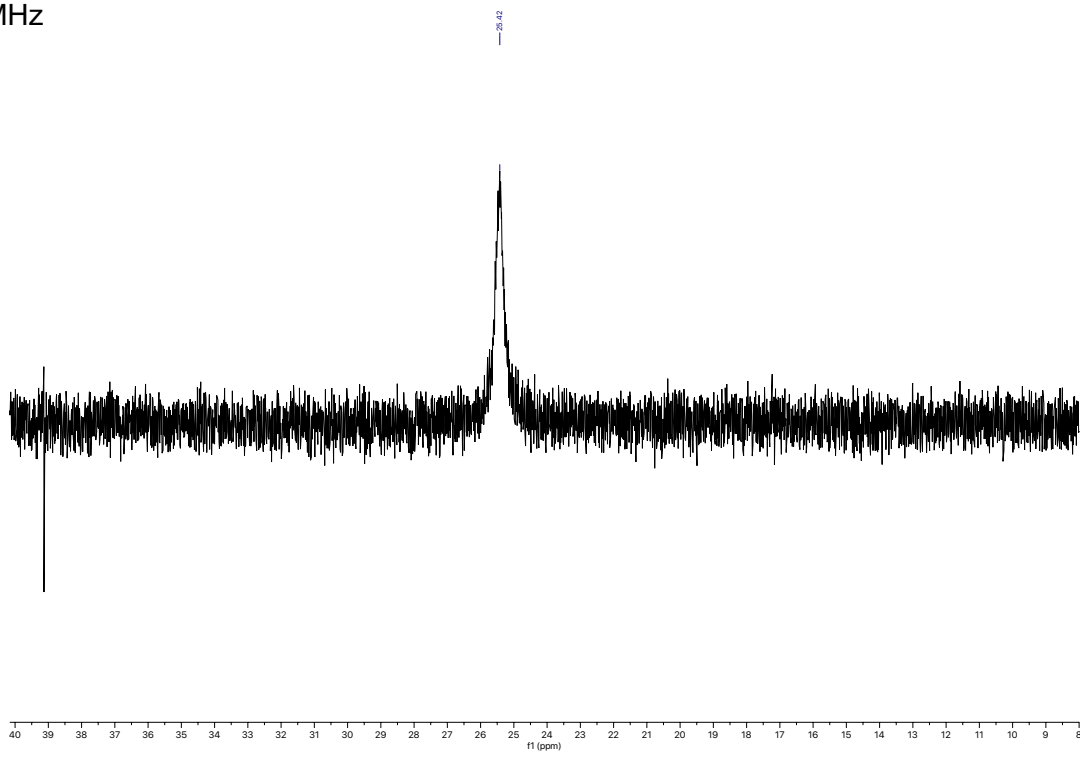

$^{1}$H NMR
600 MHz
$D_2O$

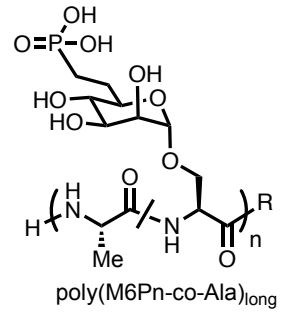


poly(M6Pn-co-Ala)$_{long}$




$^{31}$P NMR
162 MHz
$D_2O$

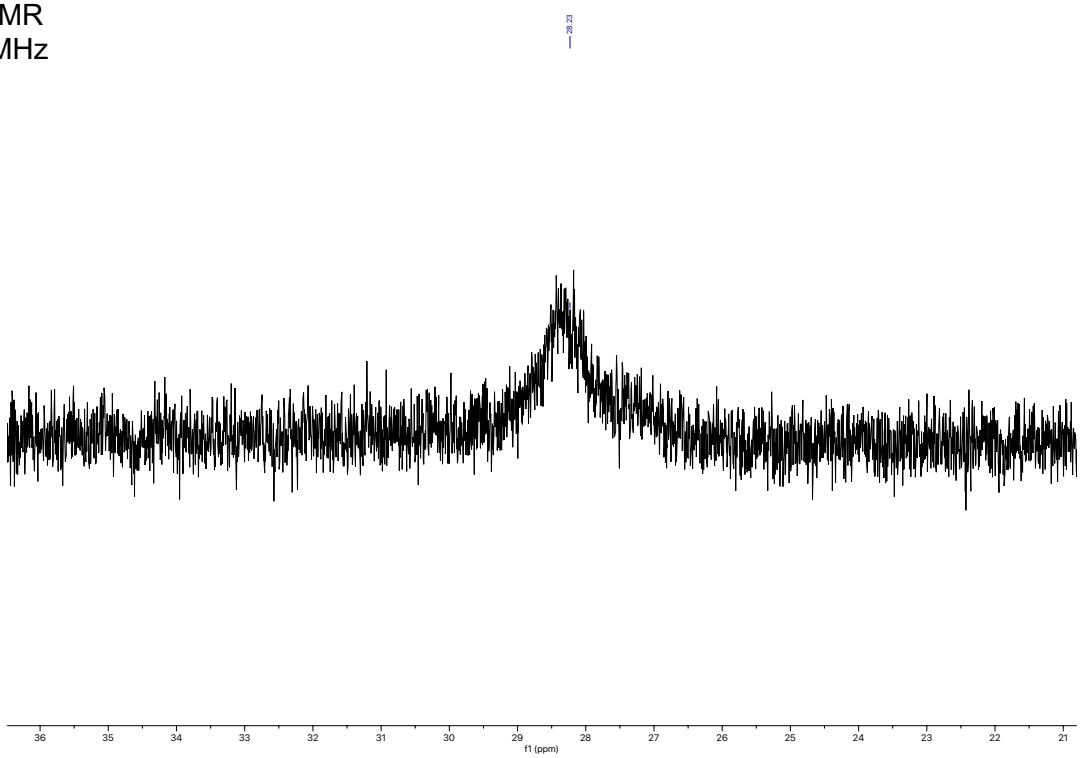

$^{1}$H NMR
600 MHz
$D_2O$

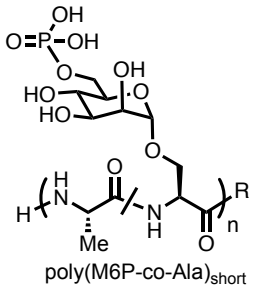


poly(M6P-co-Ala)$_{short}$




$^{31}$P NMR
162 MHz
$D_2O$

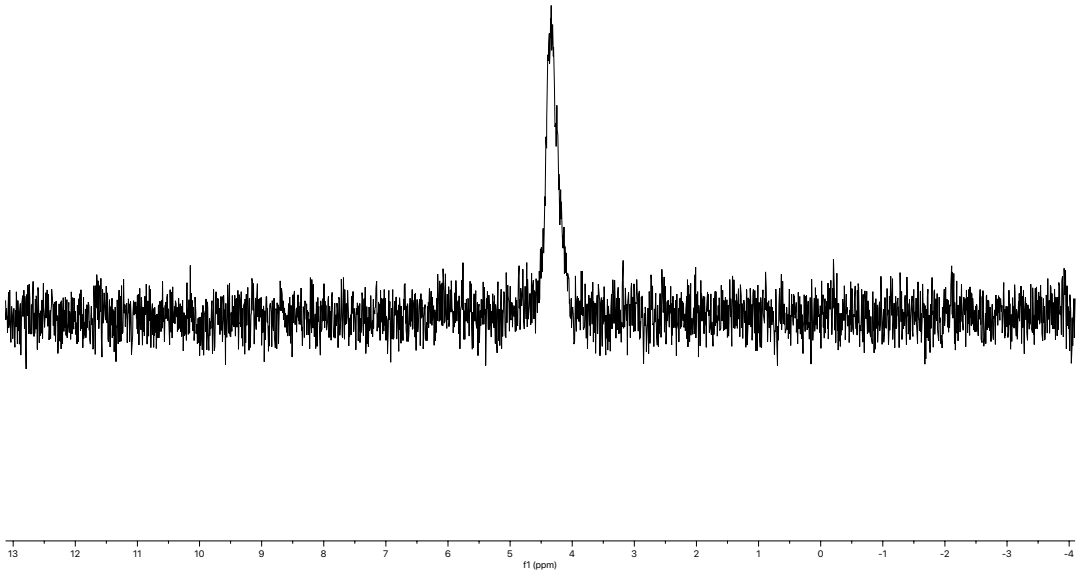

$^{1}$H NMR
600 MHz
$D_2O$

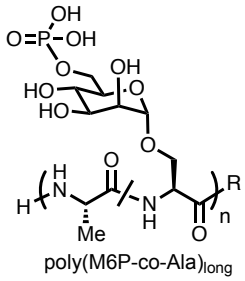


poly(M6P-co-Ala)$_{long}$




$^{31}$P NMR
162 MHz
$D_2O$